LAWRENCE
LIVERMORE
NATIONAL
LABORATORY

LLNL-TR-641530

Np(V) Sorption and Diffusion on Montmorillonite Clay Progress Report M4FT-13LL08060327

M. Zavarin, A. B. Kersting, J. D. Begg, A. Benedicto-Cordoba, P. Zhao

July 29, 2013

Disclaimer

This work performed under the auspices of the U.S. Department of Energy by Lawrence Livermore National Laboratory under Contract DE-AC52-07NA27344.

July 26, 2013

Np(V) Sorption and Diffusion on Montmorillonite Clay Progress Report M4FT-13LL08060327

M. Zavarin[a], A.B. Kersting[a], J.D. Begg[a], A. Benedicto-Cordoba[b], and P. Zhao[a]

[a]Glenn T. Seaborg Institute, Physical & Life Sciences, Lawrence Livermore National Laboratory, 7000 East Avenue, Livermore, CA 94550, USA.
[b]CIEMAT, Department of Environment, Avenida Complutense, 40, 28040 Madrid, Spain.

DISCLAIMER

Contents

1. Introduction

This progress report (Milestone Number M4FT-13LL08060327) summarizes research conducted at LLNL within Work Package Number FT-13LL080603, Disposal Research – Generic Engineered Barrier System Evaluations. The research is focused on quantifying Np(V) sorption to and diffusion through montmorillonite clay which is the primary mineralogic component of proposed bentonite backfill material in certain nuclear waste repository scenarios.

1.1 Relevance of Np to Nuclear Waste Repositories

Neptunium (Np) is a transuranic element of particular concern to the development of nuclear waste repositories. The dominant isotope, ^{237}Np, has a long half-life (2.13×10^{6} years) and high biological toxicity. In geological disposal scenarios, ^{237}Np will be one of the most radiologically significant contributors (Kaszuba and Runde, 1999; Wescott et al., 1995; Wilson et al., 1994). Dose calculations for the proposed Yucca Mountain repository suggested that Np will be a significant dose contributor at 50,000 years and the dominant dose contributor after 75,000 years (Figure 1).

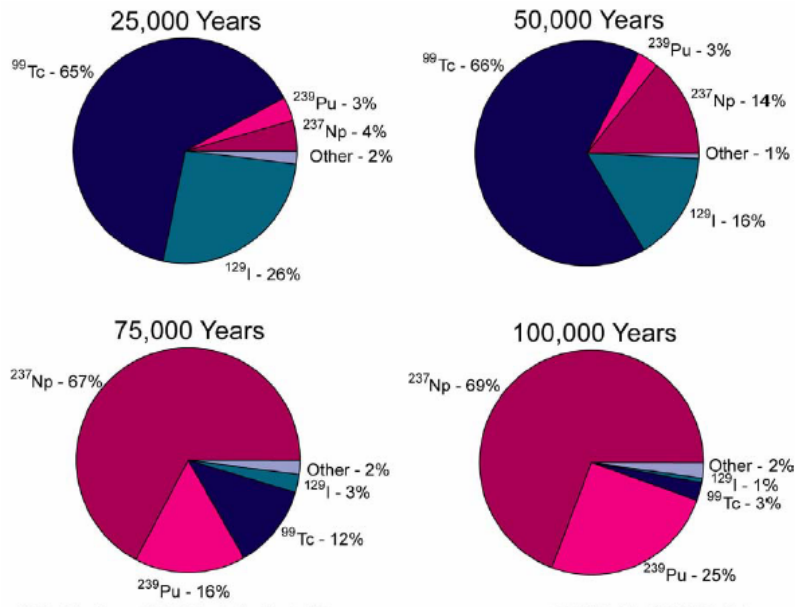

Figure 1. Fraction of mean total annual dose attributed to different radionuclides for the nominal scenario projected by the TSPA-SR model. From page 4-466, Figure 4-182 of Yucca Mountain Science and Engineering report (Doe, 2002).

In 2003, scientists at the Electric Power Research Institute re-examined the potential dose rates (Apted et al., 2003) and produced less conservative risk estimates. While the estimated dose at 10,000 years was reported to be 0 mrems per year and the dose at 1 million years was about 3 mrems per year, Np was, nevertheless, identified as the dominant radionuclide contributing to longterm dose from a nuclear waste repository (Figure 2).

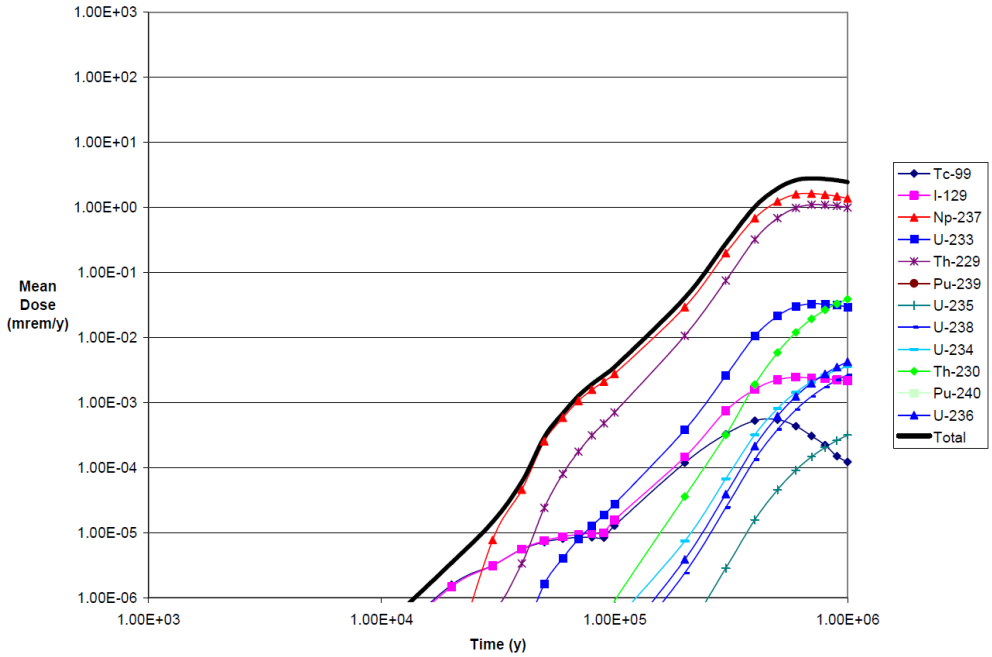

Figure 2. Annual dose attributed to different radionuclides for the IMARC 8.0, ICRP 72 dose conversion factor calculations reported in (Apted et al., 2003), page 4-18.

1.2 Np Reactive Transport

Based on our past experience at the Yucca Mountain site and elsewhere, it is apparent that a detailed understanding of Np reactive transport within engineered barrier systems (e.g. clay backfill material) as well as the surrounding natural systems is essential. The migration of Np through a repository near-field and the surrounding geosphere will be highly influenced by the nature and composition of the rock matrix. Montmorillonite is a major component of the bentonite barriers proposed in the geological nuclear waste repository designs of many countries (Dverstorp and Stromberg, 2013; Hoth et al., 2007; Nagra, 2002; Oecd, 2006). Montmorillonite may also be a dominant component of the repository host rock (e.g. Callovo-Oxfordian argillite at the French repository Cigeo) (Labalette et al., 2013). Thus, Np interaction with montmorillonite must be accurately parameterized in any performance assessment calculations.

Montmorillonite is a 2:1 smectite clay and consists of two SiO_4 tetrahedral (T) sheets bound to either side of an AlO_6 octahedral (O) sheet (expressed as T:O:T) (Dixon, 1989). Isomorphic substitutions of Al and Si give a permanent negative charge to the structure that is compensated by exchange cations. The electrostatic attraction between the charged layers and the exchangeable cations causes the cohesion of the T:O:T layers. As a result, the total cation exchange capacity is distributed between the inner surfaces in the interlayer spacing (interlamellar space) and the outer surfaces of the clay particles. In addition, the montmorillonite surface includes a pH-dependent charge associated with the broken silanol and aluminol edges of the T:O:T sheets. As a result, two mechanisms of sorption exist on montmorillonite: cation exchange at permanently charged sites and surface complexation on the variably charged silanol and aluminol edges.

The sorption of Np is controlled by both its redox and aqueous speciation (Bondietti and Francis, 1979; Kaszuba and Runde, 1999; Law et al., 2010). Under a wide range of oxic conditions, the

pentavalent oxidation state, in the form of NpO_2^+, will dominate (Choppin, 2006; Kaszuba and Runde, 1999). NpO_2^+ has a relatively low affinity to most minerals and rocks (Triay et al., 1993), resulting in its high environmental mobility.

Under aerobic conditions and at circumneutral pH values, Np(V) sorption to montmorillonite is likely to be dominated by surface complexation at the variably charged sorption sites (Bradbury and Baeyens, 2006; Turner et al., 1998b). However, at pH values below pH 6, cation exchange is expected to be the dominant sorption mechanism (Bradbury and Baeyens, 2006; Kozai et al., 1996; Nagasaki and Tanaka, 2000; Sabodina et al., 2006; Sakamoto et al., 1990; Turner et al., 1998b; Zavarin et al., 2012). Sorption by ion exchange is dependent on the composition of the clay exchange sites (Jensen, 1973), commonly occupied by Na^+, K^+, Mg^{2+} and Ca^{2+}, which is, in turn, strongly dependent on the aqueous conditions and electrolyte composition. However, most of the studies in the literature have so far focused on Np(V)-Na^+ ion exchange.

While some data are available in the literature regarding diffusion of Np(V) in clay-containing rock or compacted clay materials (e.g. (Wu et al., 2009)), the nature of the diffusion process in these clay-rich materials is not fully understood. Furthermore, the effect of temperature has been studied only minimally and is essential to exploring repository performance under increasingly high heat loads. A basic observation from various authors is that the apparent retardation measured in batch sorption experiments differs significantly from the calculated retardation based on diffusion profiles through cores. This disparity between batch and core retardation measurements was summarized by Bourg et al. (2003). They proposed an alternative model that took into account diffusion within the interparticle pore space as well as the intralamellar space (Figure 3). Predicting diffusion is further complicated by the fact that the sorption mechanism (e.g. inner sphere, outer sphere, diffuse layer) will affect diffusion rates in the interlamellar space (Figure 4).

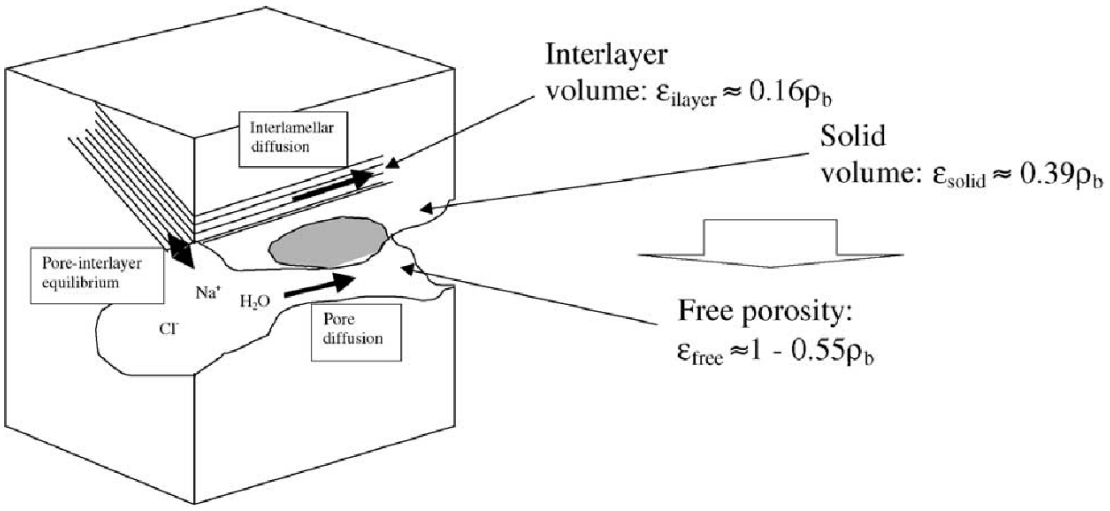

Figure 3. Example of an elementary volume of compacted bentonite, estimates of the volume fractions of interlayer porosity versus free porosity and effects on diffusion. From (Bourg et al., 2003).

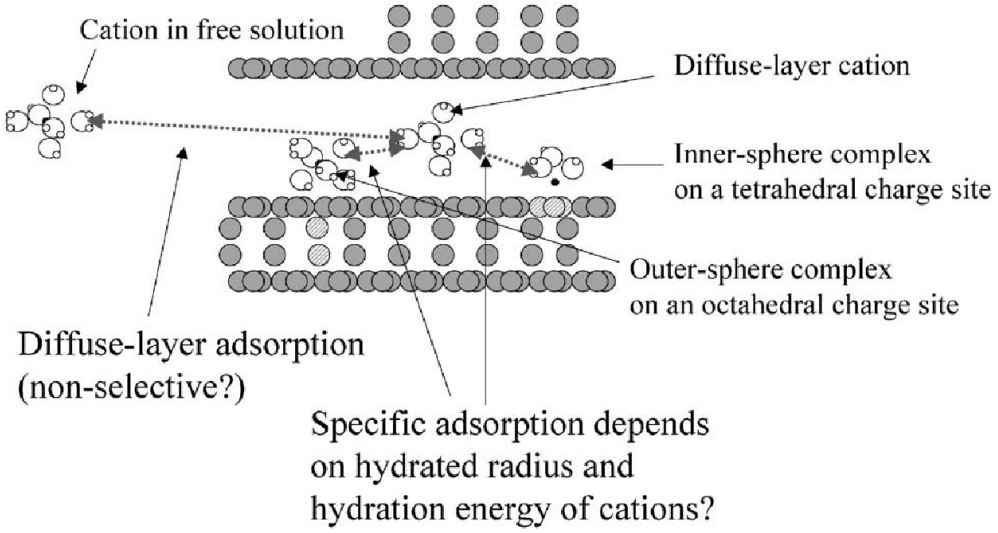

Figure 4. Example of diffuse-layer, outer-sphere, and inner-sphere interlayer adsorption processes. Each adsorption process may lead to unique diffusion rates. From (Bourg et al., 2003).

The aim of this study is to collect sorption data both experimentally and from the literature to develop a comprehensive model of Np ion exchange and surface complexation on montmorillonite. This model will be tested through a series of diffusion experiments using packed montmorillonite cores. The core diffusion experiments will examine the effect of temperature, solution conditions, and compaction on Np diffusion through an idealized montmorillonite repository backfill material and provide a dataset for detailed reactive transport model testing and calibration based on conceptual models proposed by Bourg et al. (2003) and others.

2. Development of a Np(V) Ion Exchange Model

The aim of the ion exchange study was to isolate the ion exchange mechanism of Np(V) sorption to montmorillonite. Np(V) exchange on homoionic Na, K, Ca and Mg-montmorillonite was determined experimentally at pH 4.5 using Na^+, K^+, Ca^{2+} and Mg^{2+} as electrolyte cations at ionic strengths ranging from 0.001 to 0.1 M. This experimental data was then modeled to estimate selectivity coefficients for the exchange reactions. These coefficients are essential for accurate prediction of Np mobility in reactive transport models. The experimental work described herein was extracted from a manuscript to be submitted to the Journal of Contaminant Hydrology later in FY2013.

2.1 Materials and Methods

The montmorillonite used in the experiments was SWy-1 montmorillonite (Source Clays Repository of the Clay Minerals Society). It was preconditioned and purified using the procedure reported in Zavarin et al. (2012). Briefly, the montmorillonite was (1) pre-treated in a 0.001 M HCl solution to dissolve any soluble salts, (2) reacted with a H_2O_2 solution to minimize the reducing capacity of any impurities, (3) treated in a 0.1 M NaCl solution to produce a homoionic clay suspension, (4) dialyzed in MQ H_2O (distilled−deionized water, 18.2 MΩ.cm resistivity) to remove excess salts, and (5) centrifuged at 180 g for 5 min and 2500 g for 6 hrs to remove the >2

μm and <50 nm particles from the suspension. The clay was then dried at 40 °C. The particles had a surface area of 31.5 m^2 g^{-1} which is consistent with the reported value of 31.8 m^2 g^{-1} (Clay Minerals Repository). XRD patterns were obtained on a Bruker D8 X-ray diffractometer and compared favorably with the montmorillonite. An obvious second mineral phase was not observed indicating that the prepared montmorillonite was relatively pure. Previously, a cation exchange capacity of 870 meq kg^{-1} for the SWy-1 clay has been determined by Baeyens and Bradbury (2002) using a ^{22}Na isotopic dilution method.

Stock suspensions of the K, Ca or Mg exchanged montmorillonite were prepared by dialyzing 5 g of preconditioned Na-montmorillonite in 500 mL of 0.1 M KCl, $CaCl_2$ or $MgCl_2$, respectively. The electrolyte was changed every day for a period of one week. Following homoionization, the clays were washed repeatedly with MQ H_2O to remove excess salts. For sorption experiments, suspensions of 2 g L^{-1} were prepared by diluting homoionized clays in the appropriate electrolyte at ionic strengths of 0.1, 0.01 and 0.001M.

The isotope ^{237}Np was used in batch sorption experiments. Separation of ^{237}Np from ^{233}Pa was performed using the procedure of Pickett et al. (1994). The purified solution was analyzed using a Cary 500 UV-Vis spectrophotometer and the Np(V) oxidation state was verified by observation of a single absorption band at 979 nm (Waggener, 1958). For sorption experiments, ^{237}Np stock solutions of 5×10^{-4}, 5×10^{-5}, and 5×10^{-6} M were prepared.

Np sorption isotherms were performed using the Na, K, Ca, and Mg-montmorillonite suspensions and spiking them with ^{237}Np at initial concentrations between 2×10^{-8} and 5×10^{-6} M. Experiments were carried out in polyethylene tubes containing homoionic montmorillonite suspensions at three ionic strengths: 0.1, 0.01 and 0.001M. The pH was fixed to 4.5 in order to isolate cation exchange as the unique Np(V) sorption mechanism (Zavarin et al., 2012). Given the acidity associated with the Np stock following purification, the pH was readjusted to 4.5 with dilute HCl or 0.1 M NaOH as necessary following spiking. After spiking, the tubes were sealed and placed on an orbital shaker at room temperature for 6 days which is sufficient to achieve equilibrium (Zavarin et al., 2012). Due to the acidic nature of the Np(V) spike and the need to adjust solution pHs to 4.5, solution ionic strengths increased upon addition of Np(V). However, cation concentrations were monitored in all samples so as to account for any changes in solution composition.

The ^{237}Np concentration was analyzed using a Perkin Elmer Liquid Scintillation Analyzer (LSA) model Tri-Carb 2900TR in alpha-beta discrimination mode. After the sorption period, total Np activity in the suspension ($[Np]_{tot}$) was counted to account for Np sorption to container walls. The difference between the theoretically added Np and the counted Np_{tot} was up to 13%, indicating some Np sorption to tube walls. Samples were then centrifuged at 7600 g for 2 h to achieve a < 30 nm particle size cut-off and Np activity in the supernatant ($[Np]_{sol}$) was determined. Na^+, K^+, Ca^{2+} and Mg^{2+} concentrations in the supernatant were determined by ion chromatography (IC) using a Dionex-ICS 600.

The thermodynamic database used for aqueous speciation was the NEA database including the hydrolysis and carbonate complexation constants selected by Lemire et al. (2001) and Neck et al. (1994). Activity correction was based on the Davies equation.

The distribution coefficient, K_d, was calculated by means of the following equation:

$$K_d = \frac{[\mathrm{Np}]_{tot} - [\mathrm{Np}]_{sol}}{[\mathrm{Np}]_{sol}} \frac{1}{[mont]} \quad (1)$$

where [mont] is the montmorillonite concentration in the suspension (g mL^{-1}).

In this study, Np(V) speciation, Np sorption data fitting, and ion exchange simulations were carried out using the FIT4FD code (Zavarin et al., 2004b). The FIT4FD modeling of sorption data and determination of Np ion exchange selectivity coefficients was conducted by fitting all sorption isotherms simultaneously. The FIT4FD code allowed us to account for the unique cation composition of each sample and the associated measurement uncertainties. The simultaneous fitting of all ion exchange data ensured that the resulting ion exchange constants (and their associated uncertainties) were self-consistent across the entire range of solution compositions examined. Ion exchange selectivity coefficients were determined using both the Vanselow and Gaines-Thomas conventions, as we describe in detail in the following section.

The ion exchange reaction between a cation B, with charge z_B, in the aqueous phase and a cation A, with charge z_A, at the cation exchange sites of a clay can be represented by:

$$z_B\, Clay(A) + z_A\, B^{z_B+} \leftrightarrow z_A\, Clay(B) + z_B\, A^{z_A+} \quad (2)$$

The cation exchange reaction can be described in terms of selectivity coefficients which indicate the sorption preference between two ions of different charge and size for the exchange site. An example of a calculation of the selectivity coefficient for an *A/B* exchange is shown in equation 3. In this case, selectivity coefficient values above 1 denote a higher affinity for cation *B* than for cation *A*. It should be noted that the selectivity coefficient is not a true thermodynamic exchange constant, since it has been shown to vary with factors such as the exchanger composition or the clay tactoid size (Jensen, 1973; Tournassat et al., 2011).

In the literature, various conventions are used to define selectivity coefficients. The Gaines-Thomas and the Vanselow conventions are commonly used in different speciation codes and by different authors (e.g. Gaines-Thomas convention (Bethke and Yeakel, 2009; Bolt, 1982; Bradbury and Baeyens, 2000; Bradbury and Baeyens, 2009; Maes and Cremers, 1977; Missana and García-Gutiérrez, 2007; Parkhurst and Appelo, 1999; Poinssot et al., 1999; Tournassat et al., 2007; Yariv and Cross, 1979); Vanselow convention (Bethke and Yeakel, 2009; Fletcher and Sposito, 1989; Parkhurst and Appelo, 1999; Schindler et al., 1987; Shaviv and Mattigod, 1985; Tournassat et al., 2007; Zavarin et al., 2004b)). In the case of homovalent ion exchange where $z_A = z_B$, both conventions lead to equivalent selectivity coefficients. However, in the case of heterovalent ion exchange, the two conventions are not equivalent. Following the Gaines-Thomas convention (Gaines and Thomas, 1953), the selectivity coefficient (K_{GT}) is expressed by:

$${}^{B}_{A}K_{GT} = \frac{(E_B)^{z_A}(a_A)^{z_B}}{(E_A)^{z_B}(a_B)^{z_A}} \quad (3)$$

where a_A and a_B are the activities of the cations *A* and *B* respectively, and E_A and E_B are the equivalent fractional occupancies. The equivalent fractional occupancy is defined as the equivalents of sorbed cation per unit mass of clay (eq g^{-1}) divided by the cation exchange capacity CEC (eq g^{-1}). In the Vanselow convention (Mcbride; Sposito, 1981), the selectivity coefficient (K_V) for the reaction is defined as follows:

$$ {}^{B}_{A}K_{V} = \frac{(M_B)^{z_A}(a_A)^{z_B}}{(M_A)^{z_B}(a_B)^{z_A}} \quad (4) $$

where M_A and M_B represent the mole fraction of the ion in the exchange phase. The mole fractional occupancy is defined as the moles of sorbed cation per mass (mol g^{-1}) divided by total moles in the clay exchange complex (mol g^{-1}).

2.2 Results and Discussion

2.2.1 Np(V) Speciation

The ion exchange of Np(V) will be dependent on its speciation in solution. NpO_2^+ is predicted to be the dominant aqueous species (> 94.5 %) at the pH value (4.5) and the highest ionic strength (0.1) used in these experiments. However we note that at pH 4.5 the uncharged species NpO_2Cl^0 will also be present, albeit as a minor component (< 5.5 %). For the same ionic strength, this percentage is slightly higher with divalent cation (Ca and Mg) electrolytes, due to the higher Cl^- concentration in the electrolyte. Nevertheless, the presence of NpO_2Cl^0 will not significantly affect the ion exchange behavior of Np over the range of solution compositions investigated.

2.2.2 Cation Composition of Batch Sorption Samples

Interpretation of Np ion exchange data requires consideration of the concentration of all cations in solution at equilibrium. This is important as the composition of the electrolyte varied due to adjustments in pH made to counter the acidity of the Np(V) spike addition and because the clay released trace amounts of other cations or impurities not removed during the homoionization process (Baeyens and Bradbury, 2004; Poinssot et al., 1999).

Figure 5 shows the concentrations of Na^+, K^+, Ca^{2+} and Mg^{2+} measured in solution at the end of each experiment as a function of the final Np_{sol} concentration. Significant levels of Na^+ are present in each sample in addition to the principal cation. The Na^+ concentration in solution increases with Np concentration and follows the same trend for all four sets of "homoionic" ion exchange systems. The additional Na^+ cations are an artifact of the NaOH pH adjustment step as discussed previously. The significant concentration of Na and trace amounts of other cations found in all solutions will likely impact the ion exchange behavior of Np on montmorillonite. This effect was indeed observed in the Np sorption data and is described in the following section. Accordingly, it was necessary to account for the actual fluid ion composition of each experiment when determining Np selectivity coefficients.

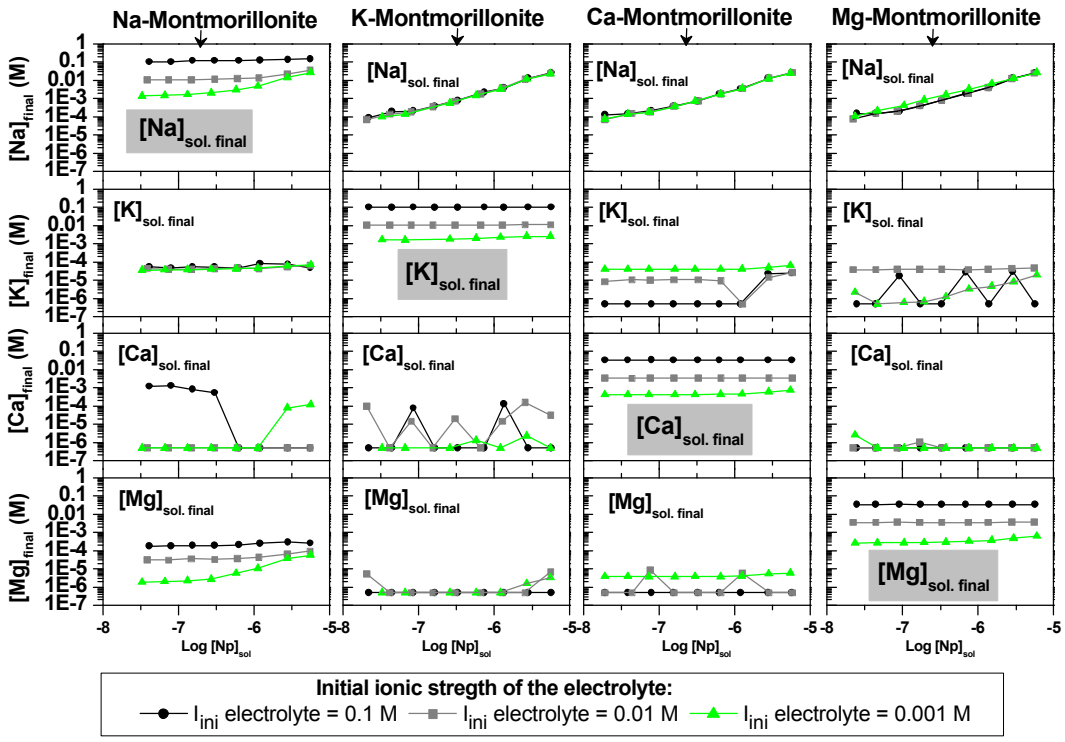

Figure 5. Cation composition of the electrolyte at the end of the experiment in the different system studied (Na, K, Ca and Mg-Montmorillonite) vs. Np loading in solution (measurements below detection limits are plotted as 5×10^{-7} M).

2.2.3 Np(V) Experimental Sorption Data

Np(V) sorption to homoionic montmorillonite (Na, K, Mg or Ca) suspended in corresponding electrolyte solutions (NaCl, KCl, $MgCl_2$ or $CaCl_2$, respectively) at three ionic strengths (0.1, 0.01 and 0.001 M) was measured over a range of initial Np concentrations (2.0×10^{-8} – 5.5×10^{-6} M). The percentage of sorbed Np as a function of the Np concentration in solution for the monovalent batch systems (Na/K-montmorillonite) and the divalent batch systems (Ca/Mg-montmorillonite) is plotted in Figure 6. There is an obvious difference in sorption behavior between Np(V) sorption in monovalent Na^+/K^+ solutions and divalent Ca^{2+}/Mg^{2+} solutions. This difference in sorption is consistent with the greater selectivity for divalent cations in montmorillonite ion exchange reactions. At low ionic strength and at low Np concentrations, the percent Np(V) sorbed in Na^+ and K^+ experiments is between 20 and 30%. This represents a K_d on the order of 137-208 mL g^{-1} which is significantly higher than the 24±5 mL g^{-1} reported by Zavarin et al. (2012) in 0.01 M NaCl which is, in turn, significantly higher than the 4-6 mL g^{-1} reported by Turner et al. (1998b) in 0.1 M $NaNO_3$. Importantly, comparison of the Turner et al. (1998b), Zavarin et al. (2012), and present data demonstrates the ionic strength dependence of Np(V) sorption at low pH and thus provides strong evidence that sorption at low pH is dominated by ion exchange processes.

As the Np concentration increases, the percent Np sorbed decreases significantly for all cation systems (Figure 6). Importantly, the trend of lower sorption with increasing Np(V) concentration initially suggested that ion exchange is limited to low Np(V) concentrations. However, as shown in Figure 5, careful examination of the background electrolyte composition indicates that the ionic strength of solutions tended to increase with the Np(V) concentration because of the acidic

nature of the Np(V) spike and the need to neutralize the solution with NaOH. Thus, the apparent decrease in Np(V) ion exchange at higher Np(V) concentrations are more correctly attributed to changes in ionic strength, as we will demonstrate in the following modeling effort.

In the monovalent experiments, increasing the ionic strength decreases the percent Np(V) adsorbed, with minimal sorption seen at the highest ionic strength (Figure 6). The low sorption at high ionic strength is consistent with Zavarin et al. (2012) who reported a K_d of <6 mL g^{-1} in 1 M NaCl solutions. Such ionic strength dependence is consistent with the ion exchange mechanisms detailed in reactions (3) and (4) which imply that the extent of sorption of a cation will be dependent on the activity of the competing cation (Langmuir, 1997).

A decrease in Np(V) sorption with increasing ionic strength is less obvious in the divalent cation experiments (Figure 6). Sorption at the lowest divalent cation ionic strength and lowest Np(V) concentration falls just above the level of detection. Thus, we can conclude that ${}^{NpO_2^+}_{Na^+}K$ and ${}^{NpO_2^+}_{K^+}K$ selectivity coefficients are significantly greater than ${}^{NpO_2^+}_{Ca^{2+}}K$ and ${}^{NpO_2^+}_{Mg^{2+}}K$ selectivity coefficients. Kozai et al. (1996) also reported lower Np(V) sorption on homoionic Ca- and Mg-montmorillonite relative to K- and Na-montmorillonite.

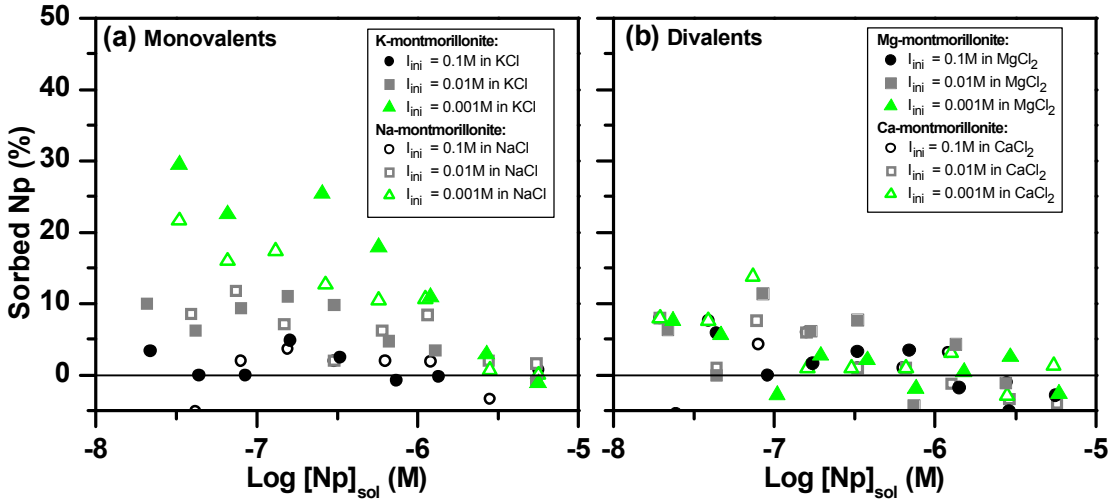

Figure 6. Percent Np sorbed to montmorillonite plotted vs. log Np concentration in solution at pH 4.5 and ionic strengths of 0.001 M, 0.01 M and 0.1 M in: (a) monovalent systems (Na/K-montmorillonite in NaCl/KCl) and (b) divalent systems (Ca/Mg-montmorillonite in $CaCl_2$/$MgCl_2$).

2.2.4 Modeling Np(V) Ion Exchange to Montmorillonite

For simple binary ion exchange experiments, the selectivity coefficient between two cations can be determined by fitting experimental data to equations 3 or 4. In the present case, this approach is not possible because exchange isotherm solution conditions vary both in ionic strength and the electrolyte cation composition. As a result, selectivity coefficients between cation pairs (e.g. ${}^{NpO_2^+}_{Na^+}K$, ${}^{NpO_2^+}_{K^+}K$, ${}^{NpO_2^+}_{Ca^{2+}}K$ and ${}^{NpO_2^+}_{Mg^{2+}}K$) cannot be fitted individually. The FIT4FD code allows for the fitting of all batch isotherm data simultaneously and can account for the measured cation composition (i.e. Na, K, Ca, Mg, and Np) of each individual sample in the fitting process. In

addition, uncertainties for each measured cation concentration can be accounted for in the minimization routine. In principle, data fitting could be performed such that selectivity coefficients, written as binary reactions, are allowed to vary simultaneously to reach a "best fit". However, in reality, this approach leads to a poorly constrained problem. In addition, this approach leads to an unintended fitting of selectivity coefficients between the major cations (e.g. ${}^{K^+}_{Na^+}K$, etc.) for which selectivity coefficients are well established in the literature. For example, if the data fitting yields $\log\left({}^{NpO_2^+}_{Na^+}K_V\right)$ and $\log\left({}^{NpO_2^+}_{K^+}K_V\right)$ selectivity coefficients of -0.34 and -0.31, respectively, it implies a $\log\left({}^{K^+}_{Na^+}K_V\right)$ selectivity coefficient of (-0.34) – (-0.31) = -0.03. However, this value contradicts the selectivity coefficient reported in the literature ($\log\left({}^{K^+}_{Na^+}K_V\right)$ = 0.26 (Fletcher and Sposito, 1989)). To minimize the number of fitting parameters in our modeling effort and ensure consistency with published ion exchange selectivity coefficients between the major cations (i.e. ${}^{K^+}_{Na^+}K$, ${}^{Ca^{2+}}_{Na^+}K$, and ${}^{Mg^{2+}}_{Na^+}K$), we limited our fitting parameter to ${}^{NpO_2^+}_{Na^+}K$ while forcing the ion exchange selectivity coefficients between Np and the other major cations to be determined based on the major cation selectivity coefficients reported in the literature (e.g. $\log\left({}^{NpO_2^+}_{K^+}K_V\right)=\log\left({}^{NpO_2^+}_{Na^+}K_V\right)-\log\left({}^{K^+}_{Na^+}K_V\right)$.

A comprehensive table of Vanselow selectivity coefficients for many major and minor cations (but not Np) and montmorillonite was published by Fletcher and Sposito (1989). The relevant selectivity coefficients used in the present modeling effort are reproduced in Table 1. Note that reactions with clay edges as proposed by Fletcher and Sposito (1989) were not included in this analysis as they were found to be insignificant at the low pH examined here. A number of publications by Bradbury and Baeyens have applied the Gaines-Thomas convention to various cation ion exchange datasets (Baeyens and Bradbury, 1995; Baeyens and Bradbury, 1997). In these models, the selectivity coefficient, $\log\left({}^{Ca^{2+}}_{Na^+}K_{GT}\right)$ was reported as 0.61. A $\log\left({}^{Mg^{2+}}_{Na^+}K_{GT}\right)$ selectivity coefficient was not reported. However, based on results from Fletcher and Sposito (1989), we assume that the Gaines-Thomas selectivity coefficient for Mg-Na ion exchange will be similar if not equivalent to Ca-Na. For homovalent ion exchange, the Vanselow and Gaines-Thomas conventions are equivalent. Thus, we use the ${}^{K^+}_{Na^+}K$ value of Fletcher and Sposito (1989) in a Gaines-Thomas model without incurring any additional uncertainty (Table 1).

Importantly, all calculated ion exchange reaction constants contain some level of uncertainty. These uncertainties are a combination of measurement uncertainty and uncertainty associated with the choice of conceptual and numerical model. For example, Tournassat et al. (2011) determined that clay tactoid size and organization will affect the apparent ion exchange properties of clays. In addition, the composition of montmorillonites from different sources can lead to differences in measured ion exchange properties. These effects are not addressed in the present modeling effort. However, it is acknowledged that the resulting Np selectivity coefficients are affected by our choice of a relatively simple conceptual model.

Table 1. Reaction constants for Na, K, Ca, and Mg ion exchange on montmorillonite based on the Vanselow and Gaines-Thomas conventions

Reaction	**Log K_V**[a]	**Log K_{GT}**[b]
Mont(Na) + $K^+ \leftrightarrow$ Mont(K) + Na^+	0.26	0.26[c]
2 Mont(Na) + $Ca^{2+} \leftrightarrow$ Mont(Ca) + 2 Na^+	0.17	0.61
2 Mont(Na) + $Mg^{2+} \leftrightarrow$ Mont(Mg) + 2 Na^+	0.17	0.61[d]

[a] Fletcher and Sposito (1989). K_a is equal to the Vanselow conditional equilibrium constant, K_V, assuming ideal mixing (i.e. activity coefficients for species on the solid phase are equal to one).
[b] Baeyens and Bradbury (1995).
[c] Based on $K_V = K_{GT}$ for homovalent ion exchange.
[d] Assumed based on similar reaction constant reported for Ca^{2+} and Mg^{2+} in the Vanselow model.

Initially, all data were fit simultaneously while allowing only the ${}^{NpO_2^+}_{Na^+}K$ selectivity coefficient to vary. All other coefficients were taken from Table 1 and the cation exchange capacity of SWy-1 was taken to be 870 meq kg^{-1} (Baeyens and Bradbury, 1997). Both the Vanselow and Gaines-Thomas conventions were tested. The resulting constants are listed in Table 2. The $\log\left({}^{NpO_2^+}_{Na^+}K\right)$ selectivity coefficients based on the Vanselow and Gaines-Thomas conventions are -0.26±0.03 and -0.14±0.04, respectively. The Np(V) selectivity coefficients with respect to K^+, Ca^{2+} and Mg^{2+} were determined (Table 2) based on the fitted ${}^{NpO_2^+}_{Na^+}K$ selectivity coefficient and the fixed major cation selectivity coefficients reported in Table 1. The ${}^{NpO_2^+}_{Na^+}K$ selectivity coefficients determined using the Vanselow and Gaines-Thomas conventions are similar, as would be expected for homovalent exchange reactions. They are also within the range of selectivity coefficients reported in previous studies for Np-Na ion exchange on smectite ($\log\left({}^{NpO_2^+}_{Na^+}K\right)$ = 0.06 to -0.75) (Bradbury and Baeyens, 2006; Gorgeon, 1994; Kozai et al., 1996; Kozai et al., 1993; Turner et al., 1998b; Zavarin et al., 2012). The slight difference in Vanselow and Gaines-Thomas selectivity coefficients is caused primarily by the differences in fixed ${}^{K^+}_{Na^+}K$, ${}^{Ca^{2+}}_{Na^+}K$ and ${}^{Mg^{2+}}_{Na^+}K$ selectivity coefficients used in the two models as shown in Table 1. Residual errors reported in the FIT4FD code as WSOS/DF (weighted sum of squares divided by the degrees of freedom) (Zavarin et al., 2004b) were 2.48 using the Vanselow convention and 2.54 using the Gaines-Thomas convention, indicating a very small improvement in the fit to the experimental data with the Vanselow convention.

Table 2. Fitted ion exchange reaction constants for Np(V) .

		Vanselow		Gaines-Thomas	
Nº free parameters		logK_V	WSOS/DF	logK_{GT}	WSOS/DF
1:	Np-Na	-0.26 (0.03)[a]	2.48	-0.14 (0.04)	2.54
	Np-K[b]	-0.52		-0.40	
	Np-Ca[b]	-0.69		-0.89	
	Np-Mg[b]	-0.69		-0.89	
2:	Np-Na K-Na	-0.34 (0.05) -0.03 (0.16)	2.43	-0.20 (0.05) 0.01 (0.17)	2.52
	Np-K[b]	-0.31		-0.21	
	Np-Ca[b]	-0.85		-1.01	
	Np-Mg[b]	-0.85		-1.01	

[a] Values in parentheses are the uncertainties in the reported values (at one standard deviation).
[b] Selectivity coefficients calculated from fitted Np-Na selectivity coefficient combined with fixed or fitted major cation selectivity coefficients.

A slightly better fit to the data can be achieved by varying the ${}^{NpO_2^+}_{Na^+}K$ and ${}^{K^+}_{Na^+}K$ selectivity coefficients simultaneously (WSOS/DF: 2.43 and 2.52 for the Vanselow and Gaines-Thomas conventions, respectively). However, the resulting ${}^{NpO_2^+}_{Na^+}K$ selectivity coefficients do not change significantly from the earlier fit (Table 2). Furthermore, the fitted $\log\left({}^{K^+}_{Na^+}K\right)$ selectivity coefficients (Vanselow: -0.03; Gaines-Thomas: 0.01) deviate significantly from the reported values in the literature (Vanselow = Gaines-Thomas: 0.26) (Table 1). Thus, it appears that adjusting selectivity coefficients for the major cations is neither necessary nor justified in this case.

Figure 7 compares the Np isotherm data (presented as K_d rather than % sorbed) to the predicted values using a Vanselow fitted $\log\left({}^{NpO_2^+}_{Na^+}K_V\right)$ selectivity coefficient (-0.26) and associated values from Table 1. Given the low Np sorption in the divalent cation systems, values for corresponding Ca^{2+} and Mg^{2+} systems are averaged and presented together in the same plot. Figure 7 demonstrates that a single ${}^{NpO_2^+}_{Na^+}K_V$ fitted selectivity coefficient is able to accurately predict Np(V) sorption to montmorillonite over the wide range solution conditions considered in this study.

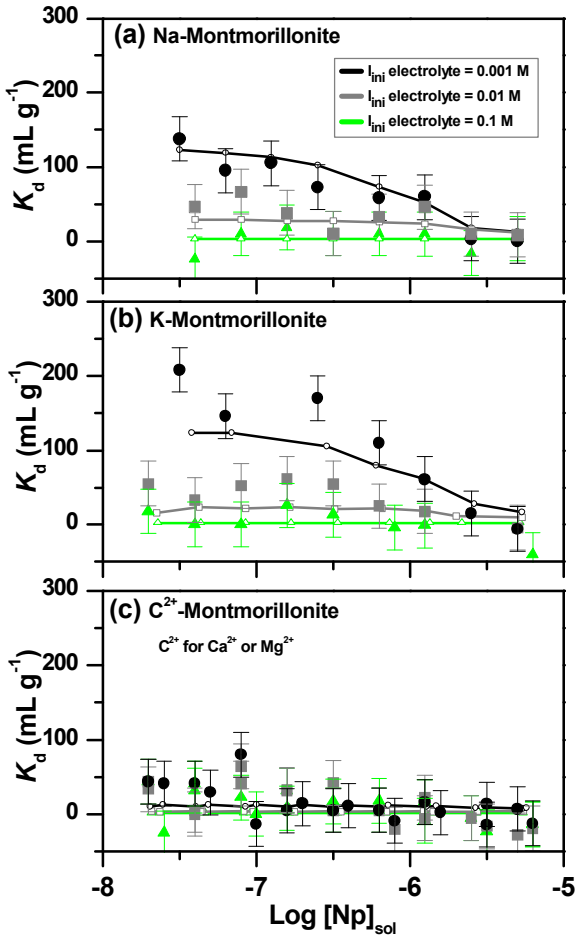

Figure 7. Experimental data (K_d) and model fit of Np(V) ion exchange (pH 4.5) on (a) Na-montmorillonite, (b) K-montmorillonite and (c) C^{2+}-montmorillonite. Predicted values based on the Vanselow convention, using parameters in Table 1 and fitted $\log\left(\frac{NpO_2^+}{Na^+}K_V\right)$ = -0.26.

2.2.5 Simulation of Np(V) Sorption to Montmorillonite

In order to illustrate the independent effect of each major cation (Na, K, Ca or Mg) on Np ion exchange on montmorillonite without interference from other cations in the electrolyte, Np sorption in mono-electrolyte solutions was simulated using the Vanselow ion exchange model (1 free parameter) developed above. Figure 8 shows the predicted K_d values over a range of cation concentrations (0.0001 - 1 M). At equivalent electrolyte cation concentration, Np sorption is lower in divalent systems (Ca^{2+} and Mg^{2+}) than in monovalent systems (K^+ and Na^+). Further, the slope of the curves is lower in divalent systems, indicating that K_d is less affected by divalent cation concentration than monovalent Na^+ or K^+ concentration.

Such behaviour is consistent with the ionic exchange mechanism. In the ion exchange processes represented in equation 2, the theoretical dependence on ionic strength can be derived from equation 1 and equation 3. When the cation adsorbate *B* is present at trace level, the dependence can be expressed as follows (Baeyens and Bradbury, 1995):

$$z_A \cdot Log(K_d) = -z_B Log[A] + Log\left(\frac{{}^{B}_{A}K_{GT}(CEC)^{z_A}\gamma_B^{z_A}}{z_B^{Z_A}\gamma_A^{Z_B}}\right) \quad (5)$$

where [A] is the concentration of the cation A in solution (M) and γ_A and γ_B are the solution activity coefficients of cations A and B. Thus, for a homovalent exchange (NpO_2^+-Na^+ or NpO_2^+-K^+) the dependence of the logarithm of the distribution coefficients (log(K_d)) with the logarithm of the concentration of the main ion of the electrolyte log[A] is represented by a line with a slope of -1. For NpO_2^+-Ca^{2+} exchange, this dependence is a line with slope -0.5, as indicated by the simulation.

A result of the dependency of Np-montmorillonite exchange on ionic strength shown in Figure 8, is that high K_d values could be reached in waters with low Na^+ and K^+ concentrations and in the absence of divalent cations. For example, in waters with [Na] or [K] of 10^{-4} M, K_d values of 3800 mL g^{-1} and 2400 mL g^{-1} may be achieved. However, such conditions are not characteristic of typical natural waters.

It should be stressed that in these simulations (Figure 8) the intention was to focus solely on the ion exchange component. As a result, the contribution of surface complexation reactions to the overall K_d was not addressed. Turner et al. (1998) predicted much higher K_d values for Np sorption on montmorillonite in 0.1 M $NaNO_3$ electrolyte (100 to 1000 mL g^{-1}) than observed in the current simulations because of the contribution of Np(V) surface complexation. For a true estimation of total Np sorption (by ionic exchange and also by surface complexation), pH, anion composition, and redox conditions must also be taken into account.

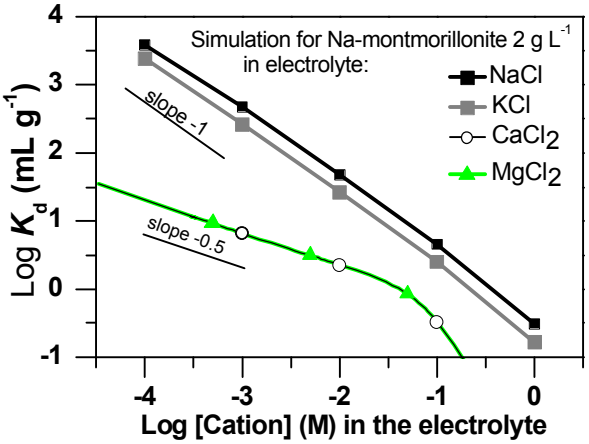

Figure 8. Simulation of Np(V) ionic exchange on montmorillonite (2 g L^{-1}) at pH 4.5 in pure electrolyte (NaCl, KCl, $MgCl_2$ and $CaCl_2$) for $[Np]_{total}$ = 5 x 10^{-7} M. Predicted values with Vanselow convention, using parameters in Table 1 and fitted Np-Na LogK_V = -0.26.

2.3 Summary

The experimental data obtained in this study indicate that Np ionic exchange highly depends on the major cation composition of the aqueous system, being especially limited by the presence of divalent cations such as Ca^{2+} and Mg^{2+} in solution. In many geochemical scenarios under medium-acid pH conditions, Np(V) migration-retention can be highly influenced by NpO_2^+ ionic

exchange on montmorillonite, which is a mineral ubiquitous in the environment. At basic conditions, ionic exchange becomes less significant and surface complexation of Np(V) will dominate.

A sorption model was developed on the basis of the experimental data, which is consistent with selectivity coefficients reported in the literature for the exchange between major cations on montmorillonite. The recommended selectivity coefficients for Np(V) ionic exchange on montmorillonite, according to the Vanselow convention, are as follows: $\log\left({}^{NpO_2^+}_{Na^+}K_V\right) = -0.26$, $\log\left({}^{NpO_2^+}_{K^+}K_V\right) = -0.52$, $\log\left({}^{NpO_2^+}_{Ca^{2+}}K_V\right) = -0.69$, $\log\left({}^{NpO_2^+}_{Mg^{2+}}K_V\right) = -0.69$. Their use in geochemical computer codes will allow better predictions of the Np(V) behaviour in the environment.

3. Development of a Np(V) Surface Complexation Model

In modeling radionuclide migration in the environment, distribution coefficients (K_d) are often used to model sorption. K_ds are typically reported as the ratio of total sorbed concentration (mol/g) to total aqueous concentration (mol/mL). Although the K_d approach can adequately describe the sorptive behavior of a particular sediment at a particular pH and solution composition, many factors that affect radionuclide sorption in geochemically dynamic environments cannot be accounted for. Surface complexation (SC) and ion exchange (IE) reactions provide a more mechanistic approach to modeling sorption and can account for the effect of changing environmental conditions on sorption. In this section, Np(V) sorption to aluminosilicate minerals is modeled using a non-electrostatic surface complexation model (NEM). Surface complexation is modeled using a generalized approach in which surface complexation to aluminosilicate >SiOH or >AlOH reactive sites is considered equivalent to the reactivity of aluminum oxide and silica reactive sites. The work presented in this section is a continuation of surface complexation modeling and database development efforts conducted at LLNL over the past decade (Zavarin and Bruton, 2004a; Zavarin and Bruton, 2004b; Zavarin et al., 2004a; Zavarin et al., 2012; Zavarin et al., 2005).

Minerals that exhibit variable surface charge (e.g. goethite, calcite, montmorillonite, etc.) can significantly reduce radionuclide mobility in the environment. The reduced mobility is partly a result of surface complexation (SC) reactions: reactions involving mineral surface functional groups and aqueous species. A typical SC reaction and associated equilibrium constant can be written in the following manner:

$$>SiOH + NpO_2^+ \Leftrightarrow >SiONpO_2 + H^+ \quad (6)$$

$$K = \frac{(>SiONpO_2)(H^+)}{(>SiOH)(NpO_2^+)} \quad (7)$$

where >SiOH is a surface functional group, NpO_2^+ is an aqueous species that reacts with the surface (to form $>SiONpO_2$), and H^+ is released as a result of the reaction. Just as for simple aqueous complexation reactions, the above SC reaction has an equilibrium reaction constant, K, that describes the relative activity of all species at equilibrium.

Factors that influence radionuclide surface complexation on a particular mineral and, thus, affect

radionuclide migration include:

- Surface area
- pH
- Aqueous complexation
- Ionic strength
- Surface electrical charge

Since SC reactions occur at the mineral-water interface, surface complexation will be a function of the mineral surface area available for reaction. The pH can significantly affect surface complexation as well. For example, in equation 6, as the concentration of H^+ increases, a larger fraction of NpO_2^+ will remain in solution. Surface functional groups (e.g. >SiOH) may also become protonated/deprotonated as a function of pH which will affect surface complexation. Aqueous complexation will influence the concentration of aqueous species in solution; this will also affect surface complexation. For example, neptunium surface complexation decreases as a function of carbonate concentration in solution due to the formation of neptunyl carbonate complexes (neptunyl carbonate complexes remain primarily in the aqueous phase). Ionic strength may influence surface complexation by reducing the activity of aqueous species. Surface complexes as well as surface protonation and deprotonation may alter the electric double layer of the surface which can, in turn, influence surface complexation..

There are many models that describe surface complexation (non-electrostatic, constant capacitance, diffuse layer, triple layer, and others). Unlike the electrostatic models, the non-electrostatic model (Kurbatov et al., 1951) does not account for surface electrical charge and its effect on sorption. The electrostatic models typically contain one or more parameters that account for surface charge effects. Although the NEM approach over-simplifies the factors affecting surface complexation, several investigators have used this model approach to describe surface complexation (Bradbury and Baeyens, 1997; Davis et al., 1998; Zachara, 1995). Davis et al. (1998) argued that the NEM may be the most appropriate for complex environmental applications since the surface charging behavior of non-ideal natural mineral phases is not well known. In this report, this most simplified model is used to quantify radionuclide sorption and simulate radionuclide migration.

3.1 Non-Electrostatic Surface Complexation Model Development

Fitting NEM reactions to radionuclide sorption data was accomplished with the fitting program FITEQL (Herbelin and Westall, 1994). Data were typically retrieved from published sorption data using the Datathief 1.0.8 program (Huysen and Van Der Laan, 1992). While fitting the data, ionic strength, pH, and aqueous complexation were taken into account while electrostatic effects were ignored. The effect of ionic strength on ion activity was accounted for by the Davies equation. Aqueous complexation constants were based on the GEMBOCHS thermodynamic database version data.com.V8.R6 (Johnson and Lundeen, 1997). Note that Np(V) speciation constants from this database vary slightly from that used in the ion exchange model calibration (Lemire et al., 2001). All data will be fitted to a common speciation model at a later date.

Several authors have shown that sorption of radionuclides to aluminosilicate minerals can be related to surface complexation on alumina and silica surfaces since surface functional groups are comparable (Mckinley et al., 1995; Turner et al., 1996). In the following sections, this generalized aluminosilicate NEM model is used to fit published radionuclide-aluminosilicate

sorption data. Although the assumption that all >AlOH or >SiOH surface reactive sites are equivalent irrespective of the mineral substrate can only be defended in a very qualitative manner, the results presented below indicate that the relationship does hold true in many cases. Nevertheless, caution must be exercised when attempting to extrapolate generalized >AlOH and >SiOH NEM constants to aluminosilicate minerals for which data is not available. The equivalent reactivity of various aluminosilicate minerals should only be used as a validation effort for available data and extrapolation should only be attempted in a hypothetical manner.

In order to retain the most simplified approach to describing the reactive sites on aluminosilicate minerals, several simplifying assumption were made. These assumptions were held constant for all sorption data fits so as to produce a consistent set of NEM reactions. A single type of >SiOH and/or >AlOH reactive site was used to fit each data set. For all minerals, a site density of 2.31 sites/nm^2 was used. Dzomback and Morel (1990) used this site density for surface complexation modeling of hydrous ferric oxide surfaces. Turner (1995) also used this site density for a variety of minerals to minimize the number of fitting parameters and arrive at a uniform set of surface complexation reactions; this same approach is taken here.

The acidity constants used for >AlOH and >SiOH surface reactive sites were taken from SiO_2 and α-Al_2O_3 diffuse layer model fits reported by Turner (1995). Depending on the SC model, surface acidity Log K constants can vary drastically. The diffuse layer model acidity constants were chosen for convenience. If acidity constants were varied during data fitting along with radionuclide surface complexation constants, less variability in Log K constants might be achieved. However, the limited data for most radionuclide–mineral sorption reactions do not merit additional fitting parameters in our NEM model.

McKinley et al. (1995) determined from transmission electron microscopy (TEM) measurements that SWy-1 montmorillonite broken edge sites (those that account for >SiOH and >AlOH sites) account for ~30% of the measured BET surface area (assuming 2.31 sites/nm^2). Turner et al. (1996) reported similar values from particle size and crystallographic data but chemical methods resulted in much higher site concentrations. Several authors have used a surface complexation reactive site density equivalent to 10% of total BET surface area to model montmorillonite sorption results (Bertetti et al., 1998; Pabalan et al., 1998; Turner et al., 1998b). Their site density was based on potentiometric titration results of Wanner et al.(1994). Bertetti et al. (1998) used the same reduced effective surface area to account for reduced Np(V) sorption to clinoptilolite relative to quartz and α-alumina. In the following aluminosilicate fits to sorption data, 10% of BET surface area was used for all montmorillonite and clinoptilolite data fits. For all sorption fits, the pKa's for >SiOH and >AlOH sites were also held constant. This minimized the number of fitting parameters and resulted in a consistent set of surface complexation reactions.

For each Np(V)–mineral pair, NEM reaction constants are reported based on average fits to all available sorption data sets. However, fits to certain data sets were omitted from the database average when the quality of sorption data was questionable. The process of data rejection is rather subjective. Nevertheless, justification for data rejection is reported in the following section.

Table 3. Summary of reaction constants developed for Np(V) surface complexation to aluminosilicate minerals.

Sorption Type	Element Conc.	Sorption Sites	Ionic Strength	pCO_2	Species	log K	Comments	Refs.
	--------	mol/l --------						
Np(V) on colloidal alumina	1E-14	9.97E-5	0.1	3.5	$>AlONpO_2$	-2.31	pH curve	1
					$>AlONpO_3H^-$	-13.59		
	1E-14	9.97E-5	0.1	0.05M	$>AlONpO_2$	-2.18	pH curve	1
					$>AlONpO_3H^-$	-10.19		
	1E-14	9.97E-5	0.1	3.5	$>AlONpO_2$	-2.18	pH curve	2
					$>AlONpO_3H^-$	-13.65		
	6E-6	6.71E-4	0.1	3.5	$>AlONpO_2$	-2.49	pH curve	4
					$>AlONpO_3H^-$	-13.62		
Np(V) on α-Al_2O_3	6E-6	9.59E-6	0.1	3.5	$>AlONpO_2$	-4.36	pH curve	4
					$>AlONpO_3H^-$	-14.21		
	1E-6	3.53E-6	0.01	none	$>AlONpO_2$	-4.78	pH curve	5
					$>AlONpO_3H^-$	-14.27		
	1E-6	3.53E-6	0.01	none	$>AlONpO_2$	-4.86	pH curve	5
					$>AlONpO_3H^-$	-14.29		
	1.9E-7	4.6-6.4E-7	0.01	5E-5	$>AlONpO_2$	-2.52	pH curve	3
					$>AlONpO_3H^-$	-12.84		
	1.9E-9	4.6-6.4E-7	0.01	5E-5	$>AlONpO_2$	-2.74	pH curve	3
					$>AlONpO_3H^-$	-12.44		
Np(V) on SiO_2	1E-14	8.05E-4	0.1	3.5	$>SiONpO_2$	-5.31	pH curve	2
					$>SiONpO_3H^-$	-12.90		
	1E-7	4.6E-6	0.1	3.5	$>SiONpO_2$	-3.59	pH curve	5
					$>SiONpO_3H^-$	-11.77		
	1E-7	9.2E-6	0.1	3.5	$>SiONpO_2$	-3.74	pH curve	5
					$>SiONpO_3H^-$	-11.59		
	1E-6	4.6E-6	0.1	3.5	$>SiONpO_2$	-3.90	pH curve	5
					$>SiONpO_3H^-$	-12.06		
	1E-6	4.6E-6	0.1	none	$>SiONpO_2$	-3.82	pH curve	5
					$>SiONpO_3H^-$	-12.03		
	1E-6	7.67E-6	0.1	none	$>SiONpO_2$	-3.56	pH curve	5
					$>SiONpO_3H^-$	-12.29		
Np(V) on clinoptilolite	1E-6	2.33E-6 (Al), 1.32E-5 (Si)	0.1 0.1	3.5 none			average fit	5
	1E-6	4.65E-6 (Al), 2.64E-5 (Si)	0.01 0.01	3.5 none				
Np(V) on montmorillonite	9.25E-7	7.66E-5 (Al,Si)	0.1	3.5			average fit	6
	9.13E-7	7.59E-5 (Al,Si)	0.1	none				

REFERENCES: 1. (Righetto et al., 1988); 2. (Righetto et al., 1991); 3. (Allard et al., 1982); 4. (Nakayama and Sakamoto, 1991); 5. (Bertetti et al., 1998); 6. (Turner et al., 1998)

3.2 Np(V) on Aluminum Oxide

Several authors have examined the interaction of Np(V) with aluminum oxide minerals (Allard et al., 1982; Bertetti et al., 1998; Nakayama and Sakamoto, 1991; Righetto et al., 1991; Righetto et al., 1988). Sorption experiments were performed on both colloidal and larger particle size Al_2O_3. Sorption experiments performed on colloidal material resulted in very low surface loading. During fitting, it was found that fitted NEM constants determined for colloidal and larger particle sorption experiments differed significantly. Np(V) sorbed more strongly to colloidal aluminum oxide even when surface area differences were accounted for. This difference may be indicative of surface structural differences between the two forms of aluminum oxide which may lead to differences in Np(V) affinities for these surfaces. Regardless of the underlying mechanisms, average NEM Log K constants were calculated for high and low surface area sorbing materials separately. Fitted NEM constants for each data set are listed in Table 3. Average NEM database constants (Table 4) were based on the low surface area aluminum oxide minerals.

Model results using average fitted NEM constants for colloidal aluminum oxide experiments are shown in Figures 9 to 12. For nearly all colloidal aluminum oxide sorption data, best fit Log K constants are quite similar resulting in a good match between the average Log K constants model results and data. The average values are -2.37 ± 0.55 and -13.62 for $>AlONpO_2$ and $>AlONpO_3H^-$, respectively. A standard deviation for the $>AlONpO_3H^-$ NEM constant could not be determined because it is an average of two values; its effect on sorption is significant only at very high pH where data are limited. Figure 10 shows the data and fit to sorption experiments conducted in 0.05 mol/L $NaHCO_3$. In this case, the data fit is poor. Inadequate control of carbonate alkalinity in these experiments may, in part, have led to the poor fit. However, the underestimated sorption at high pH may also be indicative of formation of ternary Np(V)-carbonate surface complexes. The limited data available are not sufficient to justify additional NEM reactions.

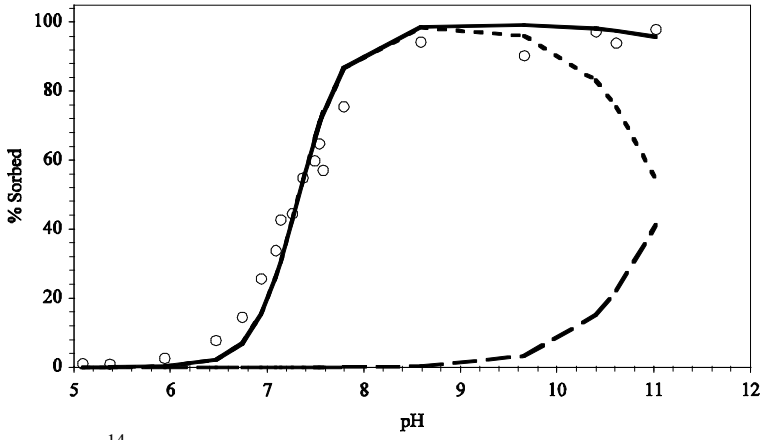

Figure 9. Sorption of 10^{-14} mol/L Np(V) on colloidal alumina. Solid lines represent data fits using average colloidal alumina NEM constants. Dashed lines represent contribution of $>AlONpO_2$ (short dash) and $>AlONpO_3H^-$ (long dash) to sorption. I = 0.1; 0.2 g/L Al_2O_3; 130 m^2/g Al_2O_3; open to air; data from Righetto et al.(1988).

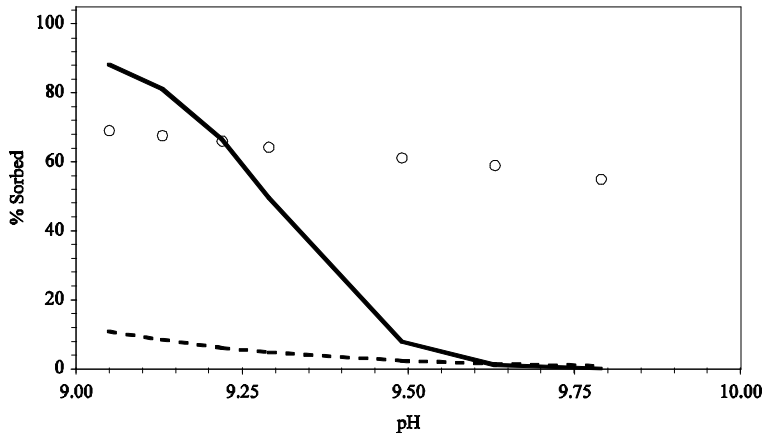

Figure 10. Sorption of 10^{-14} mol/L Np(V) on colloidal alumina. Solid lines represent data fits using average colloidal alumina NEM constants. Model fits produced assuming 0.05 mol/L HCO_3^- (solid line) or atmospheric CO_2 (dashed line); I = 0.1; 0.2 g/L Al_2O_3; 130 m^2/g Al_2O_3; open to air; data from Righetto et al. (1988).

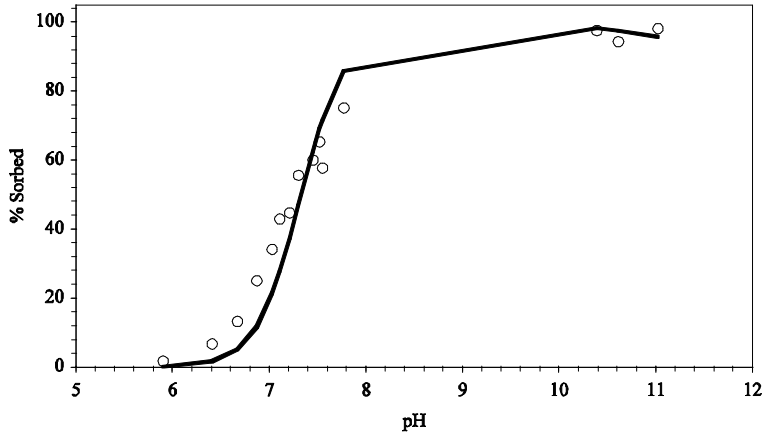

Figure 11. Sorption of 10^{-14} mol/L Np(V) on colloidal alumina. Solid line represents data fit using average colloidal alumina NEM constants. I = 0.1; 0.2 g/L Al_2O_3; 130 m^2/g Al_2O_3; open to air; data from Righetto et al. (1991).

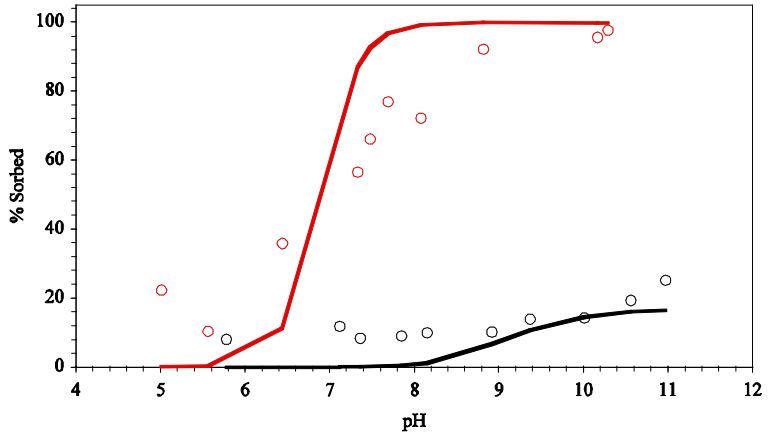

Figure 12. Sorption of 6×10^{-6} mol/L Np(V) on colloidal alumina (175 m^2/g) (red) and low surface area α-alumina (2.5 m^2/g) (black). Solid lines represent data fits using average colloidal alumina and α-alumina NEM constants. I = 0.1; 1 g/L Al_2O_3; open to air; data from Nakayama and Sakamoto (1991).

Several authors examined the sorption of Np(V) on aluminum oxide material of low surface area and relatively high surface loads (Allard et al., 1982; Bertetti et al., 1998; Nakayama and Sakamoto, 1991). The best fit NEM constants to data of Nakayama and Sakamoto (1991) and Bertetti et al. (1998) (Table 3 and Figures 12 and 13) are in good agreement. The best fit NEM constant to data of Allard et al. (1982) (Table 3 and Figure 14) is significantly higher. Since surface areas for these experiments were estimated from sieving results, it is likely that surface area estimates were too low, resulting in unusually high NEM constants. Ignoring the data of Allard et al. (1982), the average Log K constants for low surface area aluminum oxide data were estimated to be -4.67 ± 0.27 and -14.26 ± 0.04 for $>AlONpO_2$ and $>AlONpO_3H^-$, respectively.

The difference in NEM constants for the low surface area and high surface area aluminum oxide minerals is indicative of possible multiple-site binding on the aluminum oxide surface or differenes in surface characteristics of colloidal and crystalline α-Al_2O_3. However, the available data is rather limited. The lower NEM constants fit aluminosilicate sorption data suggesting that they may be more appropriate for modeling montmorillonite behavior. They are, therefore, reported in Table 4.

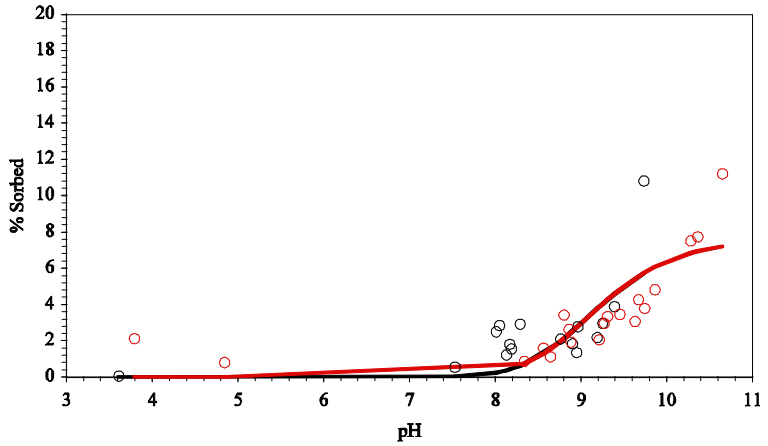

Figure 13. Sorption of 10^{-6} mol/L Np(V) on low surface area α-Al_2O_3 (two data sets). Solid lines represent data fits using average low surface area α-Al_2O_3 NEM constants. I = 0.01; 4 g/L Al_2O_3; 0.23 m^2/g Al_2O_3; in the absence of CO_2; data from Bertetti et al. (1998).

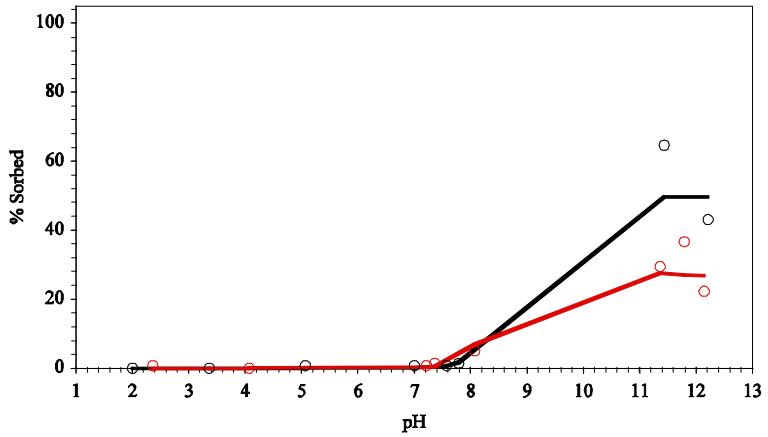

Figure 14. Sorption of 1.9×10^{-7} (red) and 1.9×10^{-9} (black) mol/L Np(V) on alumina. Solid lines represent data fits using best fit NEM constants. I = 0.01; 20 g/L alumina; 0.09-0.125 mm particle diameter; open to air; data from Allard et al. (1982).

3.3 Np(V) on Silica

Np(V) sorption to silica was examined by Righetto et al. (1991) and Bertetti et al. (1998) (Figures 15 to 17). The fitted NEM constants for the data of Righetto et al. (1991) are significantly lower than fitted NEM constants for the data of Bertetti et al. (1998) (Table 3). For the data of Righetto et al. (1991), an overestimated colloidal silica surface area could account for the low fitted NEM constant. This same pattern was observed with respect to fitted Am(III) NEM constants for the data reported by these same authors. The multiple data sets of Bertetti et al. (1998) all resulted in similar fitted NEM constants (Table 3). The average Log K constants using these data fits are –3.72±0.15 and –12.16 for $>SiONpO_2$ and $>SiONpO_3H^-$, respectively. An error estimate could not be performed for $>SiONpO_3H^-$ because this surface species contributed to sorption only when

CO_2 was absent from solutions. Only two data sets were reported by Bertetti et al (1998) at low CO_2(g).

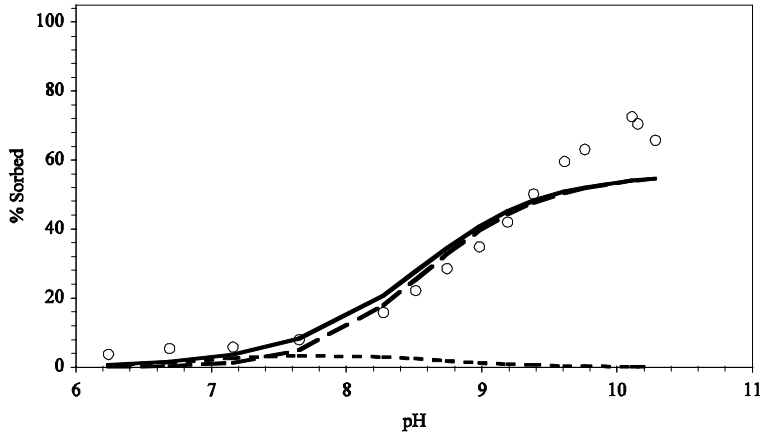

Figure 15. Sorption of 10^{-14} mol/L Np(V) on colloidal silica. Solid lines represent data fits using best fit NEM constants. Dashed lines represent contribution of individual surface species. I = 0.1; 1.2 g/L SiO_2; 175 m^2/g SiO_2 from Turner (1995); open to air; data from Righetto et al. (1991).

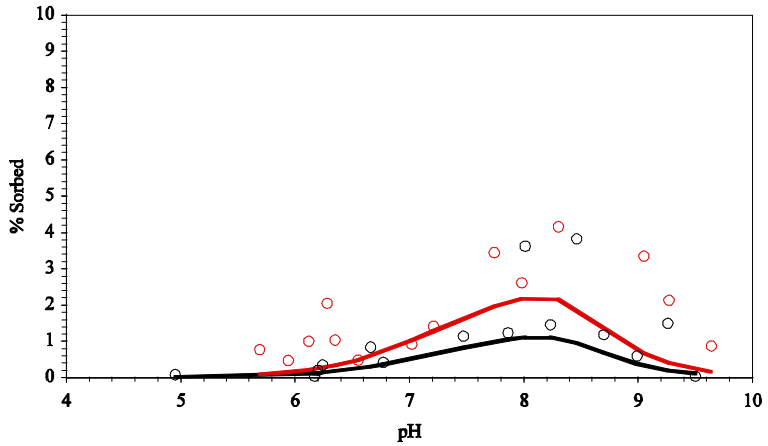

Figure 16. Sorption of 10^{-7} mol/L Np(V) to 40 g/L (black) and 80 g/L (red) SiO_2. Solid lines represent model prediction using NEM constants from Table 4. I = 0.1; 0.03 m^2/g SiO_2; open to air; data from Bertetti et al. (1998).

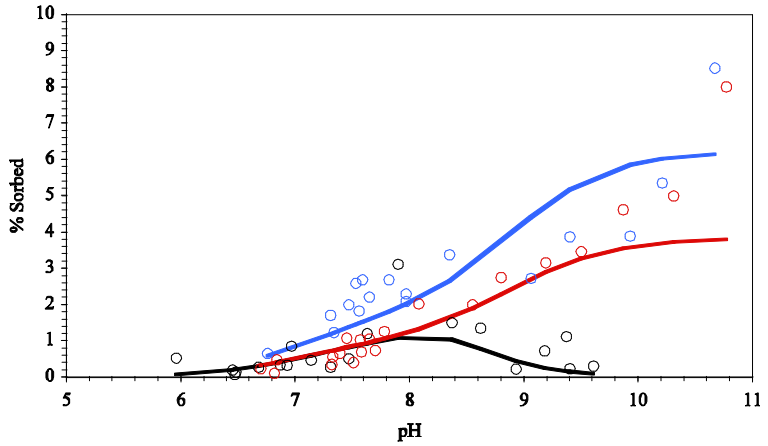

Figure 17. Sorption of 10^{-6} mol/L Np(V) on 40 g/L SiO_2 in air (black), 40 g/L SiO_2 w/o CO_2 (red), and 4 g/L fine grained SiO_2 w/o CO_2 (blue). Solid lines represent model prediction using NEM constants from Table 4. I = 0.1; 0.03 m^2/g SiO_2; 0.5 m^2/g fine grained SiO_2; data from Bertetti et al. (1998).

3.4 Np(V) on Aluminosilicates

Several authors have examined the interaction of Np(V) with aluminosilicates (Bertetti et al., 1998; Bertetti et al., 1995; Turner et al., 1998a). Turner et al. (1998a) hypothesized that Np(V) sorption to montmorillonite could be described by surface complexation to >AlOH and >SiOH sites at the edges of this layered clay mineral. Here, model results using average NEM constants determined for aluminum oxide and silica sorption experiments are compared to montmorillonite sorption data. Following the suggestion of Turner et al.(1998a), it was estimated that 10% of the BET surface area comprised reactive edge sites. Turner et al. (1998a) used an Al/Si reactive site ratio of 0.83:1; in our case, we used a ratio of 1:1. Data fits are shown in Figure 18. No adjustment of NEM constants was performed. Because two sets of NEM constants were calculated for aluminum oxides (colloidal and low surface area), fits to montmorillonite data were examined with both sets of values. Only the low surface area aluminum oxide constants fit montmorillonite data well even though surface loads on montmorillonite were relatively low. At I = 0.1, sorption at low pH was minor; indicating that ion exchange of Np(V) on montmorillonite was not significant under these experimental conditions. At lower ionic strength, ion exchange will become significant, as described in the previous section.

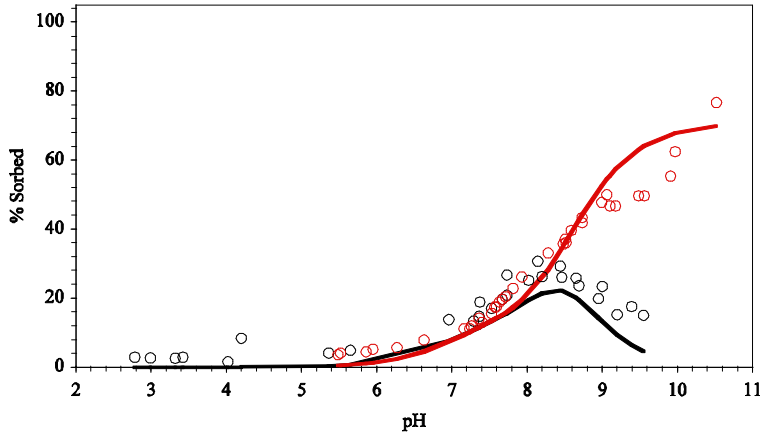

Figure 18. Sorption of ~9×10^{-7} mol/L Np(V) on montmorillonite in air (black) and w/o CO_2 (red). Solid lines represent model prediction using NEM constants from Table 4. I = 0.1; ~4 g/L montmorillonite; 97 m^2/g; 10% edge sites; 1:1 Si:Al site ratio; data from Turner et al. (1998a).

Sorption of Np(V) to clinoptilolite was evaluated in the same manner as for montmorillonite. Again, reactive surface sites were estimated to comprise 10% of the BET surface area. This new site density was determined from comparisons made by Bertetti et al. (1998) that showed clinoptilolite sorption to be equivalent to that of montmorillonite (on a surface area basis). The Al:Si reactive site ratio was estimated by the molar ratio of these elements in clinoptilolite. Pabalan (1994) measured the concentration of Al and Si in the clinoptilolite used in the experiments of Bertetti et al.(1998). The Al:Si ratio was found to be approximately 15:85, typical of clinoptilolites in general. This ratio was used to estimate the concentration of >AlOH and >SiOH reactive sites on the clinoptilolite surface. Results are presented in Figure 19. As in the case of Np(V) on montmorillonite, ion exchange under these experimental conditions was not significant, though a small amount of sorption at low pH was evident. Surprisingly, this relatively simple approach to surface complexation modeling adequately fit the observed sorption of Np(V) to clinoptilolite without any adjustment to the reaction constants independently developed for Np(V) sorption to alumina and silica.

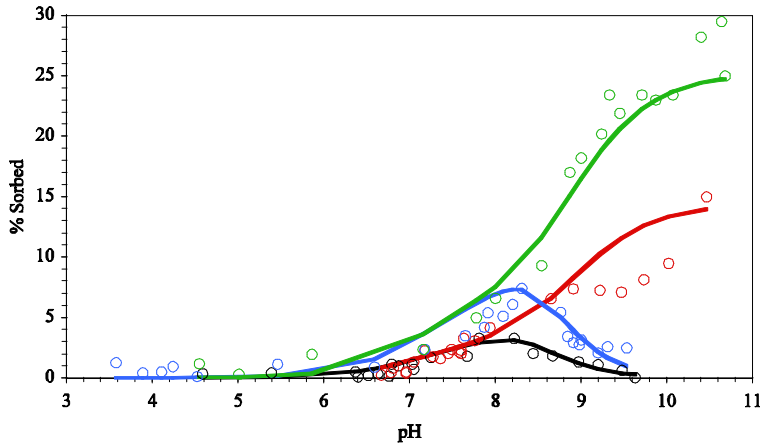

Figure 19. Sorption of 10^{-6} mol/L Np(V) on clinoptilolite with 4 g/L, I = 0.1, in air (black), 4 g/l, I = 0.1, w/o CO_2 (red), 8 g/L, I = 0.01, in air (blue), and 8 g/L, I = 0.01, w/o CO_2 (green). Solid lines represent model prediction using NEM constants from Table 4. 10.1 m^2/g clinoptilolite; 10% reactive edge sites; 15:85 Al:Si site ratio; data from Bertetti et al. (1998).

3.5 Summary

Table 4 lists the average NEM constants that comprise a database of surface complexation reactions on aluminosilicate minerals. The acidity constants used for >AlOH and >SiOH surface reactive sites were taken from SiO_2 and α-Al_2O_3 diffuse layer model fits reported by Turner (1995). Depending on the SC model, surface acidity Log K constants can vary drastically. If acidity constants were varied during data fitting along with radionuclide surface complexation constants, less variability in Log K constants might be achieved. However, the limited data for most radionuclide–mineral sorption reactions do not merit additional fitting parameters in our NEM model.

Table 4. Average non-electrostatic surface complexation model constants for Np(V) sorption to aluminosilicates.

Reaction	# of Curves Evaluated	log K	Ref.
$>AlOH \Leftrightarrow >AlO^- + H^+$		-9.73*	
$>AlOH + H^+ \Leftrightarrow >AlOH_2^+$		8.33*	
$>SiOH \Leftrightarrow >SiO^- + H^+$		-7.20*	
$>AlOH + NpO_2^+ \Leftrightarrow >AlONpO_2 + H^+$	9	-4.67±0.27	1-5†
$>AlOH + NpO_2^+ + H_2O \Leftrightarrow >AlONpO_3H^- + 2H^+$		-14.26±0.04	
$>SiOH + NpO_2^+ \Leftrightarrow >SiONpO_2 + H^+$	6	-3.72±0.15	2, 4
$>SiOH + NpO_2^+ + H_2O \Leftrightarrow >SiONpO_3H^- + 2H^+$		-12.16	

* Surface acidity constants taken from Turner (1995) SiO_2 and α-Al_2O_3 diffuse layer surface complexation model data.
† 2 montmorillonite curves and 4 clinoptilolite curves fit using average aluminol/silanol sites (refs. 13 and 14).
REFERENCES: 1. (Righetto et al., 1988); 2. (Righetto et al., 1991); 3. (Allard et al., 1982); 4. (Nakayama and Sakamoto, 1991); 5. (Bertetti et al., 1998).

The NEM constants in Table 4 are valid only when they are used in conjunction with the listed acidity constants. In addition, all NEM constants are dependent on the aqueous speciation constants used to model the data. This is particularly important for actinides and lanthanides for which aqueous speciation can be very complex. Aqueous complexation constants were based on the GEMBOCHS thermodynamic data base version data.com.V8.R6 (Johnson and Lundeen, 1997).

Sorption of Np(V) to aluminum oxide, silica, and aluminosilicate minerals using a generalized NEM approach, in combination with Vanselow IE has been accomplished using a combination of new experimental data and a survey of data from the literature. Results indicate that generalized >SiOH and >AlOH reactive sites can be used to describe sorption on a variety of minerals. Although this generalized approach may result in greater uncertainty in mineral sorption constants (when compared to a mineral-dependent model), the number of equations necessary to describe sorption is minimized. This approach also minimizes the number of fitting parameters while retaining the principal pH, ionic strength, and surface loading effects.

The NEM and Vanselow IE constants described here are an attempt to arrive at a consistent simplified database of sorption constants that can be used in reactive transport simulations in chemically heterogeneous environments. The accuracy of the resulting equations is limited by the quality and quantity of available sorption data and the limitations of the generalized NEM approach used. The reactivity of natural minerals is complicated and cannot be assumed to behave ideally. Thus, the validity of the NEM and Vanselow IE constants must always be evaluated with respect to the mineralogy and solution conditions of interest.

4. Comprehensive Approaches to Developing Ion Exchange and Surface Complexation Models for Nuclear Waste Repository Conditions

To date, we have taken the approach of developing a non-electrostatic surface complexation model in combination with ion exchange to simulate Np(V) sorption to montmorillonite. A combination of new experimental data and sorption data from the literature were used to quantify reaction constants that describe all available sorption data. This model provides the foundation for examining Np(V) diffusive reactive transport through montmorillonite clay. The compilation of raw sorption data will also allow us to test alternative approaches (new aqueous speciation models, alternative surface complexation models, uncertainty analyses) to modeling sorption. The need to develop self-consistent surface complexation/ion exchange models, in concert with thermodynamic models, for nuclear waste repository performance assessment was identified many years ago (Bradbury and Baeyens, 1993). However, significant progress on this issue has been been made only recently in various international nuclear waste repository programs (e.g. (Bradbury and Baeyens, 2009), (Dresden-Rossendorf, 2013), (Geckeis et al., 2013)). Hybrid approaches have also been attempted (Bradbury et al., 2010). The best path forward for developing such databases remains an open question (Geckeis et al., 2013), particularly in cases where generic repositories are being investigated resulting in a need to model radionuclide behavior over a very broad range of solution and mineralogic conditions.

One promising effort underway in Germany is the development of an open source database of surface complexation constants reported in the open literature (Dresden-Rossendorf, 2013). RES³T is a digital open source thermodynamic sorption database. It is mineral-specific and can therefore also be used for additive models of more complex solid phases such as rocks or soils.

The database includes an integrated user interface to access selected mineral and sorption data and export data into formats suitable for other modeling software. Data records comprise mineral properties, specific surface areas, characteristics of surface binding sites and their protolysis, sorption ligand information, and surface complexation reactions. The database includes the following suface complexation models: Non-Electrostatic, Diffuse Double Layer, Constant Capacitance, Triple Layer, Basic Stern, and the 1-pK Model as extended to CD-MUSIC. The concept of strong and weak binding sites is also included. An extensive bibliography is included in the database, providing links to the original publications, but also to background information concerning surface complexation model theories, related software for data processing and modeling, and sorption experiment techniques. The intent of the database is help to substitute the present Kd approach in risk assessment studies to the more realistic description of sorption phenomena with SCM. The RES³T approach represents the first international attempt to produce a digital thermodynamic database for surface complexation equilibria from the vast amount of data available in the literature.

As an example, a query of Np(V) sorption to aluminosilicate minerals yields the output shown in Table 5. The majority of the Np(V) surface complexation constants available in the database are associated with the Diffuse Double Layer (DDL) model. However, some NEM surface complexation constants are reported and can be compared to values reported in Section 3. For example, the NEM logK reaction constant for formation of $>SiONpO_2$ on the silanol reactive site reported to be -4.3 in the RES^{3}T and compares well with our fitted value (Table 4, -3.72±0.15). The comparison is not as promising for the aluminol reactive site $>AlONpO_2$ (-3.6 to -3.4 in RES^{3}T compared to -4.67±0.27 in Table 4). However, it should be noted that our analysis indicated that Np(V) sorption to aluminum oxides may depend on the mineral phase present (e.g. $Al(OH)_3$ vs. α-Al_2O_3, Table 3).

One significant difficulty in directly utilizing reaction constants supplied in the RES^{3}T database is that reported constants are dependent on the specific surface complexation model used in the referenced manuscript and the associated protonation/deprotonation constants, surface areas, site densities, and associated aqueous speciation constants and activity correction methods. This inconsistent application of surface complexation models in the literature limits our ability to develop self-consistent databases that would be directly applicable to reactive transport modeling efforts. Ideally, raw sorption data would be stored in a database from which one could develop surface complexation reaction constants based on preferred SCM modeling approaches and most up to date aqueous speciation databases. UFD program at LLNL is actively engaged with the RES^{3}T group to evaluate options for a next generation RES^{3}T database.

Table 5. Surface complexation reaction constants extracted from the RES^{3}T database for Np(V) sorption to aluminosilicate minerals.

SCM	Mineral	Area m2/g	SiteDensity sites/nm2	pK_1	pK_2	logK	Chemical Equation	Literature Reference
DDL	Biotite	8	2.31		7.2	2.86	»Si-OH + NpO2<1+> = »Si-OH-NpO2<1+>	TS96
DDL	Kaolinite	24.5	2.31		7.2	4.09	»Si-OH + NpO2<1+> = »Si-OH-NpO2<1+>	WAT01b
DDL	Montmorillonite	9.7	1.257		7.2	4.05	»Si-OH + NpO2<1+> = »Si-OH-NpO2<1+>	TPB98a
DDL	Montmorillonite	97	2.31		7.2	3.04	»Si-OH + NpO2<1+> = »Si-OH-NpO2<1+>	WAT01b
DDL	Biotite	7.5	2.31		7.2	-4.17	»Si-OH + NpO2<1+> = »Si-O-NpO2 + H<1+>	WAT01b
DDL	amorphous Silica	175	2.31		7.2	-12.54	»Si-OH + NpO2<1+> + H2O = »Si-O-NpO2(OH)<1-> + 2 H<1+>	WAT01b
DDL	Biotite	8	2.31		7.2	-11.58	»Si-OH + NpO2<1+> + H2O = »Si-O-NpO2(OH)<1-> + 2 H<1+>	TS96
DDL	Clinoptilolite	10.1	2.31		7.2	-13.2	»Si-OH + NpO2<1+> + H2O = »Si-O-NpO2(OH)<1-> + 2 H<1+>	WAT01b
DDL	Biotite	8	2.31	8.33	9.73	4.15	»Al-OH + NpO2<1+> = »Al-OH-NpO2<1+>	TS96
DDL	Boehmite	175	2.31	6.85	9.05	3.89	»Al-OH + NpO2<1+> = »Al-OH-NpO2<1+>	WAT01b
DDL	Diaspore	0.11	2.31	8.33	9.72	5.5	»Al-OH + NpO2<1+> = »Al-OH-NpO2<1+>	WAT01b
DDL	Gibbsite	0.22	2.31	6.85	9.05	4.95	»Al-OH + NpO2<1+> = »Al-OH-NpO2<1+>	WAT01b
DDL	Clinoptilolite	10.1	2.31	8.33	9.73	3.27	»Al-OH + NpO2<1+> = »Al-OH-NpO2<1+>	WAT01b
DDL	Boehmite	175	2.31	6.85	9.05	-4.5	»Al-OH + NpO2<1+> = »Al-O-NpO2 + H<1+>	WAT01b
DDL	Diaspore	0.11	2.31	8.33	9.72	-3.62	»Al-OH + NpO2<1+> = »Al-O-NpO2 + H<1+>	WAT01b
DDL	Gibbsite	0.22	2.31	6.85	9.05	-3.53	»Al-OH + NpO2<1+> = »Al-O-NpO2 + H<1+>	WAT01b
DDL	Gibbsite	0.8	2.31	8.33	9.73	-2.81	»Al-OH + NpO2<1+> = »Al-O-NpO2 + H<1+>	WAT01b
DDL	Kaolinite	24.5	2.31	8.33	9.73	-4.04	»Al-OH + NpO2<1+> = »Al-O-NpO2 + H<1+>	WAT01b
DDL	Alumina	130	2.31	6.85	9.05	-10.93	»Al-OH + NpO2<1+> + H2O = »Al-O-NpO2(OH)<1-> + 2 H<1+>	WAT01b
DDL	Biotite	8	2.31	8.33	9.73	-12.39	»Al-OH + NpO2<1+> + H2O = »Al-O-NpO2(OH)<1-> + 2 H<1+>	TS96
DDL	Biotite	7.5	2.31	8.33	9.72	-11.5	»Al-OH + NpO2<1+> + H2O = »Al-O-NpO2(OH)<1-> + 2 H<1+>	WAT01b
DDL	Diaspore	0.11	2.31	8.33	9.72	-13.1	»Al-OH + NpO2<1+> + H2O = »Al-O-NpO2(OH)<1-> + 2 H<1+>	WAT01b
DDL	Montmorillonite	9.7	1.043	8.33	9.73	-13.79	»Al-OH + NpO2<1+> + H2O = »Al-O-NpO2(OH)<1-> + 2 H<1+>	TPB98a
DDL	Montmorillonite	97	2.31	8.33	9.72	-13.72	»Al-OH + NpO2<1+> + H2O = »Al-O-NpO2(OH)<1-> + 2 H<1+>	WAT01b
DDL	Corundum	2.5	2.31	8.33	9.73	-8.23	2 »Al-OH + NpO2<1+> = (»Al-O)2-NpO2<1-> + 2 H<1+>	WAT01b

SCM	Mineral	Area m2/g	SiteDensity sites/nm2	pK_1	pK_2	logK	Chemical Equation	Literature Reference
DDL	Corundum	0.24	2.31	8.33	9.73	-8.23	2 »Al-OH + NpO2<1+> = (»Al-O)2-NpO2<1-> + 2 H<1+>	WAT01b
DDL	Montmorillonite	50	0.74673	6.05	7.79	1.33	»X-OH + NpO2<1+> + CO3<2-> = »X-O-NpO2CO3<2-> + H<1+>	TNOYS10
DDL	Montmorillonite	50	0.74673	6.05	7.79	2.85	»X-OH + NpO2<1+> = »X-OH-NpO2<1+>	TNOYS10
DDL	Montmorillonite	50	0.74673	6.05	7.79	-14	»X-OH + NpO2<1+> + H2O = »X-O-NpO2(OH)<1-> + 2 H<1+>	TNOYS10
NE	amorphous Silica	0.1	12.04409	2.72	6.18	-4.3	»Si-OH + NpO2<1+> = »Si-O-NpO2 + H<1+>	L93
NE	Gibbsite	0.8	10	5.7	9.4	-3.6	»Al-OH + NpO2<1+> = »Al-O-NpO2 + H<1+>	DBMCB98
NE	Gibbsite	0.8	10	5.92	9.4	-3.44	»Al-OH + NpO2<1+> = »Al-O-NpO2 + H<1+>	DMBC97
NE	Gibbsite	0.8	10	5.65	9.55	-3.41	»Al-OH + NpO2<1+> = »Al-O-NpO2 + H<1+>	DMBC97
NE	Montmorillonite	35	1.37647	5	9.5	-12	»X-OH + NpO2<1+> + H2O = »X-O-NpO2(OH)<1-> + 2 H<1+>	BB06
NE	Montmorillonite	35	1.37647	5	9.5	-2	»X-OH + NpO2<1+> = »X-O-NpO2 + H<1+>	BB06
TL	Quartz	6	2.31	-2.3	6.8	-6.929	»Si-OH + NpO2<1+> = »Si-O-NpO2 + H<1+>	KHL99

REFERENCES:

Bradbury MH, Bayens B (2006) Modelling sorption data for the actinides Am(III), Np(V) and Pa(V) on montmorillonite. Radiochim. Acta 94, 619-625.

Del Nero M, Ben Said K, Made B, Clement A, Bontems G (1998) Effect of pH and carbonate concentration in solution on the sorption of neptunium(V) by hydrargilite: Application of the Non-Electrostatic Model. Radiochim. Acta 81, 133-141.

Del Nero M, Made B, Bontems G, Clement A (1997) Adsorption of neptunium(V) on hydrargilite. Radiochim. Acta 76, 219-228.

Kohler M, Honeyman BD, Leckie JO (1999) Neptunium(V) sorption on hematite (a-Fe2O3) in aqueous suspension: The effect of CO2. Radiochim. Acta 85, 33-48.

Labonne N (1993): Role des matieres organiques dans les phenomenes de retention des actinides sur la silice.Ph.D.Thesis Université Paris XI-Orsay

Tachi Y, Nakazawa T, Ochs M, Yotsuji, Suyama T, Seida T, Yamada N, Yui M (2010) Diffusion and sorption of neptunium(V) in compacted montmorillonite: effects of carbonate and salinity. Radiochim. Acta 98, 711-718.

Turner DR, Pabalan RT, Bertetti FP (1998) Neptunium(V) sorption on montmorillonite: An experimental and surface complexation modeling study. Clays Clay Min. 46, 256-269.

Turner DR, Sassman SA (1996) Approaches to sorption modeling for high-level waste performance assessment. J. Contam. Hydrol. 21, 311-332.

Wang P, Anderko A, Turner DR (2001) Thermodynamic modeling of the adsorption of radionuclides on selected minerals. I. Cations. Ind. Eng. Chem. Res. 40, 4428-4443.

5. Diffusion Cell Experiments

While some data are available in the literature regarding diffusion of Np(V) in clay-containing rock or compacted clay materials (e.g. (Wu et al., 2009)), the nature of the diffusion process in these clay-rich materials is not fully understood. Furthermore, the effect of temperature has been studied only minimally and is essential to exploring repository performance under increasingly high heat loads. A focus of our experimental and modeling effort is to examine diffusion within the free pore space as well as the interlamellar space (Figure 3). The significance of Np(V) diffusion through the interlamellar space of montmorillonite will depend on the speciation of Np(V) in solution, its ability to access the interlamellar space via ion exchange processes, and the degree of clay compaction which will affect the relative abundance of interlamellar porosity versus free porosity (e.g. Figure 3). Np(V) diffusion through compacted clay will be examined at solution conditions that favor Np(V) sorption via ion exchange, that favor Np(V) sorption via surface complexation, that favor the presence of negatively charged Np(V) complexes in solution, and that favor the presence of a positively charged NpO_2^+ free ion. Each of these conditions will test the effects of interlamellar diffusion, charge exclusion, and pore connectivity which affect the apparent diffusion of Np(V) through an engineered clay barrier.

5.1 Materials and Methods

At present, instrumentation has been acquired and the appropriate experimental conditions are being explored based on our ion exchange/surface complexation model. The configuration of the diffusion cells is based on the original design by Van Loon et al. (2004) (Figure 20). The complete diffusion cell configuration during experiments is shown in Figure 21. Diffusion experiments will begin in late FY13.

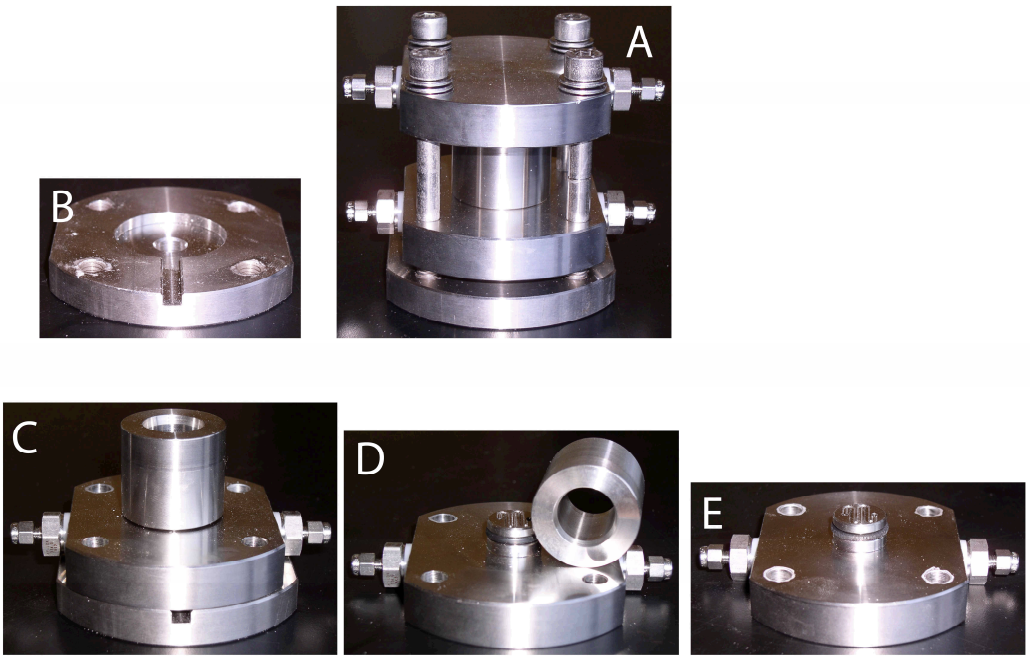

Figure 20. The diffusion cell (A) includes two ports on each side of the core to allow for continuous circulation of fluid on the upstream and downstream ends of the core. The bottom plate (B) is configured for a Burster miniature ring load sensor to monitor pressure. The central

cylinder (C and D) holds the clay core between two O-rings. Fluid circulates at the top and bottom of the core through a sinusoidal flowpath (E) that ensures a uniform concentration across the ends of the core. The top and bottom of each core is isolated between two titanium porous (2 micrometer pore size) frits. Core dimension is 18.5 mm in diameter and 10 mm in length.

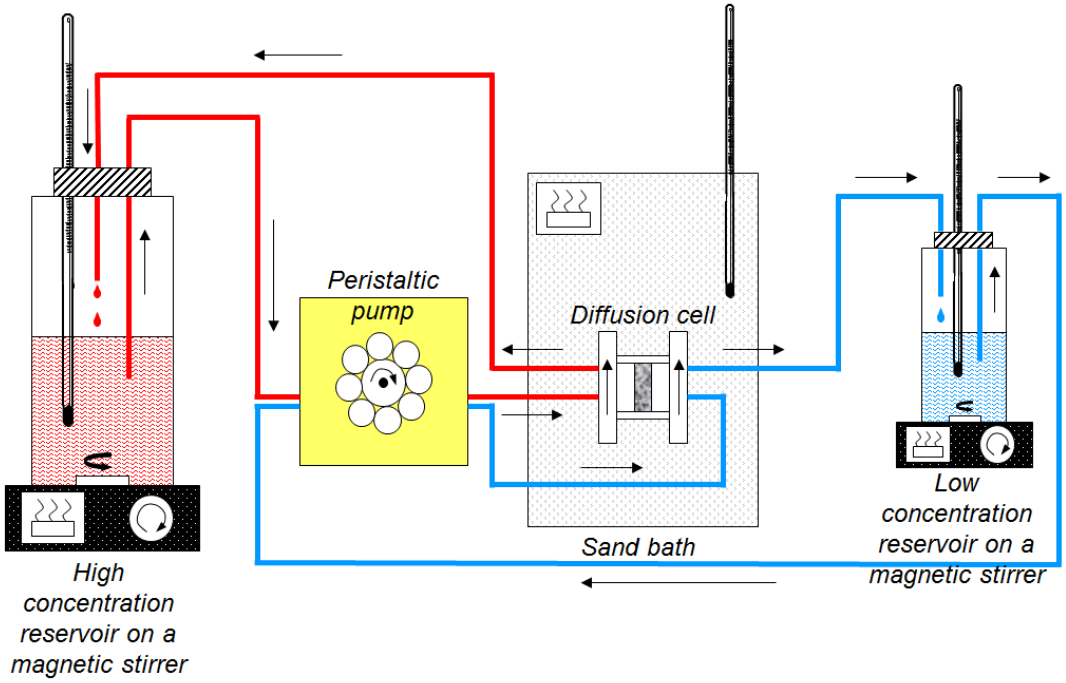

Figure 21. Configuration of diffusion cell under heated aerobic conditions. Temperature is maintain by hot plate (for reservoirs) and sand bath (for diffusion cell). Np(V) and solution composition in high concentration and low concentration reservoirs is monitored over time. If diffusion is observed across core, diffusion rate can be calculated directly. If Np(V) through diffusion is not observed, the core is disassembled and diffusion profile quantified using abrasive pealing, laser ablation ICP-MS, or secondary ion mass spectrometry (SIMS).

5.2 Characterization of Longterm Uranium Diffusion Experiments

In the Fall of 2013, a collaboration between LLNL and the Helmholtz Zentrum Dresden Rossendorf was initiated. As part of this collaboration, there was an opportunity to characterize U(VI) diffusion through compacted MX-80 bentonite cores using the same diffusion cell configuration described above (Figure 21). The unique nature of these experiments was that the diffusion cells had been allowed to run since 2006, providing an unprecedented 7 years of diffusive transport. Characterization of these samples also provided an opportunity to test various methods for characterizing core material.

Three cores were examined: compacted MX-80 bentonite with bulk densities of 1.3, 1.6, and 1.9 g/cm^3. High and low concentration reservoirs contained saline solutions that were determined to represent equilibrium composition of bentonite porewaters at their specific dry bulk densities (Table 6). The U(VI) concentration in the high concentration reservoirs was set to 1E-6 mol/L while the downstream reservoir was uranium free. Tritium diffusion through the cores was measured, leading to effective diffusities in the 1.3, 1.6, and 1.9 g/cm3 of 1.99×10^{-10}, 1.14×10^{-10}, and 4.05×10^{-11} m^2/s, respectively.

While modeling and data analysis are still ongoing, the diffusion data are indicative of a significant decrease in U(VI) migration with increasing compaction (Figure 22). Some of this is the result of a reduction in total porosity in the compacted bentonite. However, additional effects such as tortuosity and charge exclusion phenomena are likely playing a role as well. Numerical modeling of these data will provide a unique opportunity to quantify U(VI) diffusion in compacted clay over extended time periods.

Table 6. Composition of porewaters in equilibrium with MX-80 bentonite at the three bulk densities examined in these experiments.

Dry density (kg m^{-3})	1300	1600	1900
Porosity	0.122	0.044	0.019
log P_{CO_2} (bar)	-3.42	-3.47	-3.65
pH	8.00	8.00	8.00
Ionic strength (M)	0.26	0.29	0.33
Na (M)	1.83×10^{-1}	2.07×10^{-1}	2.54×10^{-1}
K (M)	2.7×10^{-3}	3.1×10^{-3}	3.7×10^{-3}
Mg (M)	1.0×10^{-2}	1.2×10^{-2}	1.5×10^{-2}
Ca (M)	9.2×10^{-3}	9.8×10^{-3}	1.2×10^{-2}
Sr (M)	8.1×10^{-5}	8.6×10^{-5}	1.1×10^{-4}
Cl (M)	1.81×10^{-2}	6.18×10^{-2}	1.70×10^{-1}
SO_4 (M)	1.02×10^{-1}	9.5×10^{-2}	7.1×10^{-2}
$C_{inorg.}$ (M)	8.9×10^{-4}	8.0×10^{-4}	5.5×10^{-4}
F (M)	2.2×10^{-4}	2.2×10^{-4}	1.9×10^{-4}
Si (M)	1.8×10^{-4}	1.8×10^{-4}	1.8×10^{-4}
N_{Na}	0.69	0.71	0.71
N_K	0.024	0.024	0.024
N_{Mg}	0.127	0.128	0.129
N_{Ca}	0.155	0.140	0.135
N_{Sr}	0.001	0.001	0.001

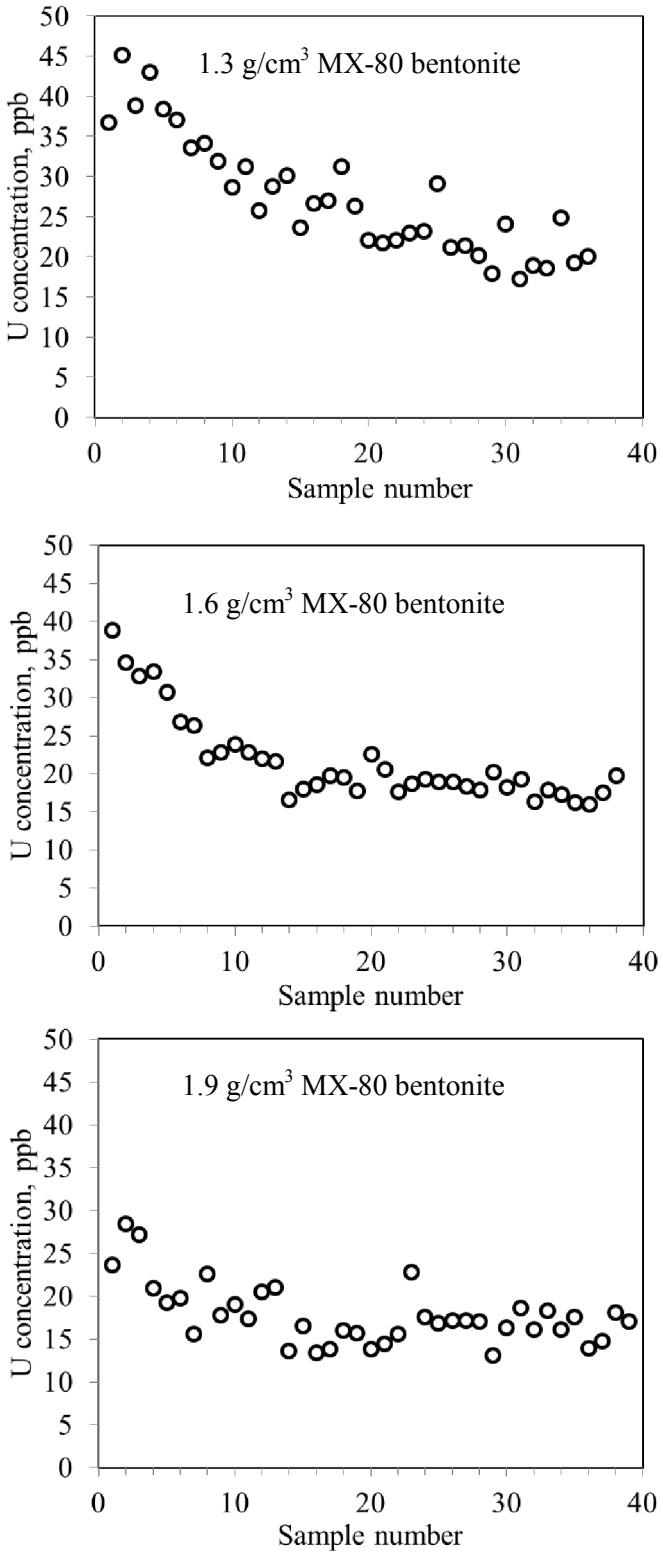

Figure 22. U(IV) diffusion profiles in compacted MX-80 bentonite cores after 7 years of diffusion. Each sample represents approximately a 100 micrometer section of core along the diffusion profile. Sample 1 is located at the high concentration side of the diffusion cell. U concentration is the desorbed U fraction in the core material after equilibration with 1 M HNO_3.

6. Planned FY14 Efforts

In FY14, we plan to continue our current experimental program looking at the diffusion of Np(V) in montmorillonite clay. At this time, the diffusion cells have been designed and made, a post doc was identified and hired, and the initial batch experiments and modeling were completed. The modeling will now focus on determining the experimental parameters needed for the diffusion cell experiments which will begin in late FY13 and continue into FY14. As data becomes available, we will be working with LBNL geochemists and modelers to provide insight into Np(V) diffusion through backfill material. We will also be working with LBNL experimentalist to compare our Np data with their parallel work on U diffusion.

We will begin FY14 effort by completing lab-scale Np diffusion experiments with compacted montmorillonite. The work will then extend to bentonite. Montmorillonite respresents a pure end-member clay while bentonite contains montmorillonite along with a variety of additional minor phases (illite, quartz, feldspar, etc.) and is more representative of what might be used in a repository environment. In addition, we are actively discussing the possibility of examining Np(V) diffusion in altered bentonite material produced hydrothermally by F. Caporuscio (Cheshire et al., 2013). This would allow us to test the diffusive properties of bentonite backfill material that may have experienced high heat loading and mineral alteration. We will employ unique x-ray spectroscopic and electron-based imaging techniques available at LBNL and LLNL to evaluate actinide diffusion on the scale of mm. The collaboration with LBNL will allow us to develop a self-consistent diffusion model for both U(VI) and Np(V).

The proposed research will address the following FEPs/needs identified in the R&D Roadmap: 2.2.09.05 - radionuclide speciation and solubility in host rock; 2.2.09.55 - sorption of dissolved radionuclides in host rock; 2.2.09.59 - colloidal transport in host rock.

7. Acknowledgments

This work was supported by the Used Fuel Disposition Campaign of the Department of Energy's Nuclear Energy Program. Prepared by LLNL under Contract DE-AC52-07NA27344.

8. References

Allard, B., Olofsson, U., Torstenfelt, B., Kipatsi, H., and Andersson, K., 1982. Sorption of actinides in well-defined oxidation states on geologic media. In: Lutze, W. (Ed.),*Scientific basis for radioactive waste management - V*. Elsevier Science Pub. Co.

Apted, M., Ross, A., and Kessler, J., 2003. Scientific and Technical Priorities at Yucca Mountain. EPRI, Palo Alto, CA.

Baeyens, B. and Bradbury, M. H., 1995. A quantitative mechanistic description of Ni, Zn and Ca sorption on Na-montmorillonite. Part II: Sorption measurements. PSI Bericht Nr. 95-11 and Nagra Technical Report NTB 95-05, Wettingen and Villigen (Switzerland).

Baeyens, B. and Bradbury, M. H., 1997. A mechanistic description of Ni and Zn sorption on Na-montmorillonite .1. Titration and sorption measurements. *J. Contam. Hydrol.* **27**, 199-222.

Baeyens, B. and Bradbury, M. H., 2004. Cation exchange capacity measurements on illite using the sodium and cesium isotope dilution technique: effects of the index cation, electrolyte concentration and competition: modeling. *Clays Clay Miner.* **52**, 421-431.

Bertetti, F. P., Pabalan, R. T., and Almendarez, M. G., 1998. Studies on neptunium(V) sorption on quartz, clinoptilolite, montmorillonite, and a-alumina. In: Jenne, E. A. (Ed.), *Adsorption of metals by geomedia*. Academic Press, San Diego.

Bertetti, F. P., Pabalan, R. T., Turner, D. R., and Almendarez, M. G., 1995. Neptunium(V) sorption behavior on clinoptilolite, quartz, and montmorillonite. In: Murphy, W. M. and Knecht, D. A. Eds.)*Materials Research Society Symposium Proceedings*. Materials Research Society, Boston, MA.

Bethke, C. M. and Yeakel, S., 2009. The Geochemist's Workbench. Release 8.0. Essentials Guide.

Bolt, G. H., 1982. *Soil Chemistry. B. Physico-Chemical Models. Chapter 2*. Elsevier.

Bondietti, E. A. and Francis, C. W., 1979. GEOLOGIC MIGRATION POTENTIALS OF TC-99 AND NP-237. *Nature* **203**, 1337-1340.

Bourg, I. C., Bourg, A. C. M., and Sposito, G., 2003. Modeling diffusion and adsorption in compacted bentonite: a critical review. *Journal of Contaminant Hydrology* **61**, 293-302.

Bradbury, M. H. and Baeyens, B., 1993. A general application of surface complexation modeling radionuclide sorption in natural systems. *J. Colloid Interface Sci.* **158**, 364-371.

Bradbury, M. H. and Baeyens, B., 1997. A mechanistic description of Ni and Zn sorption on Na-montmorillonite Part II: modelling. *J. Contam. Hydrol.* **27**, 223-248.

Bradbury, M. H. and Baeyens, B., 2000. A generalised sorption model for the concentration dependent uptake of caesium by argillaceous rocks. *J. Contam. Hydrol.* **42**, 141-163.

Bradbury, M. H. and Baeyens, B., 2002. Sorption of Eu on Na- and Ca-montmorillonites: Experimental investigations and modelling with cation exchange and surface complexation. *Geochim. Cosmochim. Acta* **66**, 2325-2334.

Bradbury, M. H. and Baeyens, B., 2006. Modelling sorption data for the actinides Am(III), Np(V) and Pa(V) on montmorillonite. *Radiochim. Acta* **94**, 619-625.

Bradbury, M. H. and Baeyens, B., 2009. Sorption modelling on illite. Part II: Actinide sorption and linear free energy relationships. *Geochim. Cosmochim. Acta* **73**, 1004-1013.

Bradbury, M. H., Baeyens, B., and Thoenen, T., 2010. Sorption Data Bases for Generic Swiss Argillaceous Rock Systems. Nagra, Wettingen, Switzerland.

Cheshire, M. C., Caporuscio, F. A., Jové-Colon, C., and McCarney, M. K., 2013. Alteration of clinoptilolite into high-silica analcime within a bentonite barrier system under used nuclear fuel repository conditions*14th International High-Level Radioactive Waste Managment Conference*. American Nuclear Society, Albuquerque, NM.

Choppin, G. R., 2006. Actinide speciation in aquatic systems. *Mar. Chem.* **99**, 83-92.

Davis, J. A., Coston, J. A., Kent, D. B., and Fuller, C. C., 1998. Application of the surface complexation concept to complex mineral assemblages. *Environmental Science and Technology* **32**, 2820-2828.

Dixon, J. B., 1989. *Minerals in Soil Environments, 2nd Edition*. Soil Science Society of America.

DOE, 2002. Yucca Mountain Science and Engineering Report: Technical Information Supporting Site Recommendation Consideration. U.S. Department of Energy, Office of Civilian Radioactive Waste Management, North Las Vegas.

Dresden-Rossendorf, H.-Z., 2013. RES³T - Rossendorf Expert System for Surface and Sorption Thermodynamics. RES³T - Rossendorf Expert System for Surface and Sorption Thermodynamics, Dresden, Germany.

Dverstorp, B. and Stromberg, B., 2013. Initial review of a license application for a spent nuclear fuel repository in Sweden*14th International High-Level Radioactive Waste Managment Conference*. American Nuclear Society, Albuquerque, NM.

Dzombak, D. A. and Morel, F. M. M., 1990. *Surface complexation modeling : hydrous ferric oxide*. Wiley, New York.

Fletcher, P. and Sposito, G., 1989. The chemical modeling of clay electrolyte interactions for montmorillonite. *Clay Min.* **24**, 375-391.

Gaines, G. L. and Thomas, H. C., 1953. Adsorption studies on clay minerals II. A formulation of the thermodynamic of exchange adsorption. *J. Chem. Phys.* **21**, 714-718.

Geckeis, H., Lützenkirchen, J., Polly, R., Rabung, T., and Schmidt, M., 2013. Mineral–Water Interface Reactions of Actinides. *Chemical Reviews* **113**, 1016-1062.

Gorgeon, L., 1994. Contribution à la Modélisation Physico-Chimique de la Retention de Radioéléments à Vie Longue par des Matériaux Argileux, Université Paris.

Herbelin, A. L. and Westall, J. C., 1994. FITEQL, A computer program for determination of chemical equilibrium constants from experimental data. Department of Chemistry, Oregon State University.

Hoth, P., Wirth, H., Reinhold, K., Bräuer, V., Krull, P., and Feldrappe, H., 2007. Endlagerung radioaktiver Abfälle in tiefen geologischen Formationen Deutschlands – Untersuchung und Bewertung von Tongesteinsformationen. BGR Bundesanstalt für Geowissenschaften und Rohstoffe, Hannover.

Huysen, K. and van der Laan, J., 1992. DataTheif. National Institute for Nuclear Physics and High Energy Physics, Amsterdam.

Jensen, H. E., 1973. Potassium–calcium exchange equilibria on a montmorillonite and a kaolinite clay. *Agrochimica* **17**, 181-190.

Johnson, J. W. and Lundeen, S. R., 1997. GEMBOCHS thermodynamic datafiles for use with the EQ3/6 modeling package. Lawrence Livermore National Laboratory, Livermore.

Kaszuba, J. P. and Runde, W. H., 1999. The aqueous geochemistry of neptunium: Dynamic control of soluble concentrations with applications to nuclear waste disposal. *Environ. Sci. Technol.* **33**, 4427-4433.

Kozai, N., Ohnuki, T., Matsumoto, J., Banba, T., and Ito, Y., 1996. A study of specific sorption of neptunium(V) on smectite in low pH solution. *Radiochim. Acta* **75**, 149-158.

Kozai, N., Ohnuki, T., and Muraoka, S., 1993. Sorption characteristics of neptunium by sodium-smectite. *J. Nucl. Sci. Technol. (Tokyo, Jpn.)* **30**, 1153-1159.

Kurbatov, M. H., Wood, G. B., and Kurbatov, J. D., 1951. Isothermal adsorption of cobalt from dilute solutions. *Journal of Physical Chemistry* **55**, 1170-1182.

Labalette, T., Harman, A., Dupuis, M. C., and Ouzounian, G., 2013. CIGÉO, the French geological repository project*14th International High-Level Radioactive Waste Managment Conference*. American Nuclear Society, Albuquerque, NM.

Langmuir, D., 1997. *Aqueous Environmental Geochemistry*. Prentice-Hall, U.S.

Law, G. T. W., Geissler, A., Lloyd, J. R., Livens, F. R., Boothman, C., Begg, J. D. C., Denecke, M. A., Rothe, J., Dardenne, K., Burke, I. T., Charnock, J. M., and Morris, K., 2010. Geomicrobiological Redox Cycling of the Transuranic Element Neptunium. . *Environ. Sci. Technol.* **44**, 8924-8929.

Lemire, R. J., Fuger, J., Nitsche, H., Potter, P., Rand, M. H., Rydberg, J., Spahiu, K., Sullivan, J. C., Ullman, W. J., Vitorge, P., and Wanner, H., 2001. *Chemical Thermodynamics of Neptunium and Plutonium*. North-Hollande by Elsevier, Amsterdam.

Maes, A. and Cremers, A., 1977. Charge density effects in ion exchange. Part 1. Heterovalent exchange equilibria. . *J. Chem. Soc. Faraday Trans.* **173**, 1807-1814.

McBride, M. B., 1994. *Environmental Chemistry of Soils* Oxford University Press, Oxford.

McKinley, J. P., Zachara, J. M., Smith, S. C., and Turner, G. D., 1995. The influence of uranyl-hydrolysis and multiple site-binding reaction on adsorption of U(VI) to montmorillonite. *Clays and Clay Minerals* **45**, 586-598.

Missana, T. and García-Gutiérrez, M., 2007. Adsorption of bivalent ions (Ca(II), Sr(II) and Co(II)) onto FEBEX bentonite. *Phys. Chem. Earth* **32**, 559-567.

Nagasaki, S. and Tanaka, S., 2000. Sorption equilibrium and kinetics of NpO_2^+ on dispersed particles of Na-montmorillonite. *Radiochim. Acta* **88**, 705-709.

NAGRA, 2002. Project Opalinus Clay. Safety Report. Demonstration of disposal feasibility for spent fuel, vitrified high-level waste and long-lived intermediate-level waste (Entsorgungsnachweis). NTB 02-05. Nagra, Wettingen, Switzerland.

Nakayama, S. and Sakamoto, Y., 1991. Sorption of neptunium on naturally-occurring iron-containing minerals. *Radiochimica Acta* **52-3**, 153-157.

Neck, V., Kim, J. I., and Kanellakopulos, B., 1994. Thermodynamisches Verhalten von Neptunium(V) in konzentrierten NaCl- und $NaClO_4$-Lösungen, Tech. Rep. Kfk 5301. Kernforschungszentrum Karlsruhe, Karlsruhe, Germany.

OECD, 2006. Safety of geological disposal of high-level and longlived radioactive waste in France—an international peer review of the "Dossier 2005 Argile" concerning disposal in the Callovo-Oxfordian formation. NEA No. 6178. OECD.

Pabalan, R. T., 1994. Thermodynamics of ion-exchange between clinoptilolite and aqueous solutions of Na+/K+ and Na+/Ca2+. *Geochimica et Cosmochimica Acta* **58**, 4573-4590.

Pabalan, R. T., Turner, D. R., Bertetti, F. P., and Prikryl, J. D., 1998. UraniumVI sorption onto selected mineral surfaces: Key geochemical parameters. In: Jenne, E. A. (Ed.), *Adsorption of metals by geomedia*. Academic Press, San Diego.

Parkhurst, D. L. and Appelo, C. A. J., 1999. User's guide to phreeqc—a computer program for speciation, batch-reaction, one-dimensional transport, and inverse geochemical calculations, USGS Report No. 99-4259.

Pickett, D. A., Murrell, M. T., and Williams, R. W., 1994. Determination of femtogram quantities of protactinium in geologic samples by thermal ionization mass spectrometry. *Analytical Chemistry* **66**, 1044-1049.

Poinssot, C., Baeyens, B., and Bradbury, M. H., 1999. Experimental studies of Cs, Sr, Ni and Eu sorption on Na-illite and the modelling of Cs sorption, PSI Bericht Nr. 99-06.

Righetto, L., Bidoglio, G., Azimonti, G., and Bellebono, I. R., 1991. Competitive actinide interaction in colloidal humic acid-mineral oxide systems. *Environmental Science and Technology* **25**, 1913-1919.

Righetto, L., Bidoglio, G., Marcandalli, B., and Bellobono, I. R., 1988. Surface interactions of actinites with alumina colloids. *Radiochimica Acta* **44/45**, 73-75.

Sabodina, M. N., Kalmykov, S. N., Sapozhnikov, Y. A., and Zakharova, E. V., 2006. Neptunium, plutonium and Cs-137 sorption by bentonite clays and their speciation in pore waters. *J. Radioanal. Nucl. Chem.* **270**, 349-355.

Sakamoto, Y., Konishi, M., Shirahashi, K., Senoo, M., and Moriyama, N., 1990. Adsorption behavior of neptunium for soil. *Radioact. Waste Manage. Environ. Restor.* **15**, 13-25.

Schindler, P. W., Liechti, P., and Westall, J. C., 1987. Adsorption of copper, cadmium and lead from aqueous solution to the kaolinite/water interface. *Neth. J. Agric. Sci.* **35**, 219-230.

Shaviv, S. and Mattigod, S. V., 1985. Cation exchange equilibria in soils expressed as cation-ligand complex formation. *Soil Sci. Soc. Am. J.* **49**, 569-573.

Sposito, G., 1981. *The Thermodynamics of Soil Solution*. Oxford University Press, Oxford.

Tournassat, C., Bizi, M., Braibant, G., and Crouzet, C., 2011. Influence of montmorillonite tactoid size on Na–Ca cation exchange reactions. *J. Colloid Interface Sci.* **364**, 443-454.

Tournassat, C., Gailhanou, H., Crouzet, C., Braibant, G., Gautier, A., Lassin, A., Blanc, P., and Gaucher, E. C., 2007. Two cation exchange models for direct and inverse modelling of solution major cation composition in equilibrium with illite surfaces. *Geochim. Cosmochim. Acta* **71**, 1098-1114.

Triay, I. R., Robinson, B. A., Lopez, R. M., Mitchell, A. J., and Overly, C. M., 1993. Neptunium retardation with tufts and groundwaters from Yucca Mountain*Proc 4th Annu Int Conf on High-Level Radioactive Waste Management.* Am. Nuclear Soc., La Grange Park, IL.

Turner, D. R., 1995. A uniform approach to surface complexation modeling of radionuclide sorption. Center for Nuclear Waste Regulatory Analyses, San Antonio.

Turner, D. R., Pabalan, R. T., and Bertetti, F. P., 1998a. Neptunium(V) sorption on montmorillonite: An experimental and surface complexation modeling study. *Clays and Clay Minerals* **46**, 256-269.

Turner, D. R., Pabalan, R. T., and Bertetti, F. P., 1998b. Neptunium(V) sorption on montmorillonite: An experimental and surface complexation modeling study. *Clays Clay Miner.* **46**, 256-269.

Turner, G. D., Zachara, J. M., McKinley, J. P., and Smith, S. C., 1996. Surface charge properties and UO22+ adsorption of a subsurface smectite. *Geochimica et Cosmochimica Acta* **60**, 3399-3414.

Van Loon, L. R. and Soler, J. M., 2004. Diffusion of HTO, $^{36}Cl^-$, $^{125}I^-$ and $^{22}Na^+$ in Opalinus Clay: Effect of Confining Pressure, Sample Orientation, Sample Depth and Temperature. Paul Scherrer Institut, Villigen PSI, Switzerland.

Waggener, W. C., 1958. Measurement of the absorption spectra of neptunium ions in heavy water solution from 0.35 to 1.85 μ. *Journal of Physical Chemistry* **62**, 382-383.

Wanner, H., Albinsson, Y., Karnl, O., Wieland, I., Wersin, P., and Charlet, L., 1994. The acid/base chemistry of montmorillonite. *Radiochimica Acta* **66/67**, 733-738.

Wescott, R. G., Lee, M. P., McCartin, T. J., Eisenberg, N. A., and Baca, R. G., 1995. NRC iterative performance assessment Phase 2: Development of capabilities for review of a performance assessment for a high-level waste repository. NUREG-1464. Nuclear Regulatory Commission, Washington, DC.

Wilson, M. L., Gauthier, J. H., Barnard, R. W., Barr, G. E., Dockery, H. A., Dunn, E., Eaton, R. R., Guerin, D. C., Lu, N., Martinez, M. J., Nilson, R., Rautman, C. A., Robey, T. H., Ross, B., Ryder, E. E., Schenker, A. R., Shannon, S. A., Skinner, L. H., Halsey, W. G., Gansemer, J. D., Lewis, L. C., Lamont, A. D., Triay, I. R., Meijer, A., and Morris, D. E., 1994. Total-system performance assessment for Yucca mountain–SLN second iteration (TSPA-1993) volume 1 and 2. SAND93-2675. Sandia National Laboratories Albuquerque

Wu, T., Amayri, S., Drebert, J., Loon, L. R. V., and Reich, T., 2009. Neptunium(V) Sorption and Diffusion in Opalinus Clay. *Environmental Science & Technology* **43**, 6567-6571.

Yariv, S. and Cross, H., 1979. *Geochemistry of Coloid Systems for Earth Sciences. Chapter 2*. Springer-Vergag.

Zachara, J. M., P.L. Gassman, S.C. Smith, and D. Taylor 1995 Oxidation and adsorption of Co(II) EDTA2− complexes in subsurface materials with iron and manganese oxides. *Geochim Cosmochim Acta* **59**, 4449-4463.

Zavarin, M. and Bruton, C. J., 2004a. A Non-Electrostatic Surface Complexation Approach to Modeling Radionuclide Migration at the Nevada Test Site: Aluminosilicates. Lawrence Livermore National Laboratory, Livermore.

Zavarin, M. and Bruton, C. J., 2004b. A Non-Electrostatic Surface Complexation Approach to Modeling Radionuclide Migration at the Nevada Test Site: Iron Oxides and Calcite. Lawrence Livermore National Laboratory, Livermore.

Zavarin, M., Carle, S. F., and Maxwell, R. M., 2004a. Upscaling Radionuclide Retardation - Linking the Surface Complexation and Ion Exchange Mechanistic Approach to a Linear Kd Approach. Lawrence Livermore National Laboratory, Livermore, California.

Zavarin, M., Powell, B. A., Bourbin, M., Zhao, P., and Kersting, A. B., 2012. Np(V) and Pu(V) Ion Exchange and Surface-Mediated Reduction Mechanisms on Montmorillonite. *Environ. Sci. Technol.* **46**, 2692-2698.

Zavarin, M., Roberts, S. K., Hakem, N., Sawvel, A. M., and Kersting, A. B., 2005. Eu(III), Sm(III), Np(V), Pu(V), and Pu(IV) sokption to calcite. *Radiochimica Acta* **93**, 93-102.

Zavarin, M., Turner, G. D., and Westall, J. C., 2004b. FIT4FD. Modification of the Program FITEQL to Facilitate Rapid Evaluation of Complex Datasets, Livermore (CA).